



저작자표시-비영리-변경금지 2.0 대한민국

이용자는 아래의 조건을 따르는 경우에 한하여 자유롭게

- 이 저작물을 복제, 배포, 전송, 전시, 공연 및 방송할 수 있습니다.

다음과 같은 조건을 따라야 합니다:



저작자표시. 귀하는 원저작자를 표시하여야 합니다.



비영리. 귀하는 이 저작물을 영리 목적으로 이용할 수 없습니다.



변경금지. 귀하는 이 저작물을 개작, 변형 또는 가공할 수 없습니다.

- 귀하는, 이 저작물의 재이용이나 배포의 경우, 이 저작물에 적용된 이용허락조건을 명확하게 나타내어야 합니다.
- 저작권자로부터 별도의 허가를 받으면 이러한 조건들은 적용되지 않습니다.

저작권법에 따른 이용자의 권리는 위의 내용에 의하여 영향을 받지 않습니다.

이것은 [이용허락규약\(Legal Code\)](#)을 이해하기 쉽게 요약한 것입니다.

[Disclaimer](#)

Master's Thesis
석사 학위논문

**Correlation Study of Surface Energy of Electrodes and
Electrolytes with Lithium Ion Battery Performance**

Hyejin Lee (이 혜 진 李 慧 眞)

Department of Energy Systems Engineering
에너지시스템공학 전공

DGIST

2016

Master's Thesis
석사 학위논문

**Correlation Study of Surface Energy of Electrodes and
Electrolytes with Lithium Ion Battery Performance**

Hyejin Lee (이 혜 진 李 慧 眞)

Department of Energy Systems Engineering

에너지시스템공학 전공

DGIST

2016

Correlation Study of Surface Energy of Electrodes and Electrolytes with Lithium Ion Battery Performance

Advisor : Professor Hochun Lee

Co-advisor : Doctor Joongoo Kang

by

Hyejin Lee

Department of Energy Systems Engineering
DGIST

A thesis submitted to the faculty of DGIST in partial fulfillment of the requirements for the degree of Master of Science in the Department of Energy Systems Engineering. The study was conducted in accordance with Code of Research Ethics¹

12.05. 2015

Approved by

Professor Hochun Lee _____ (Signature)
(Advisor)

Doctor Joongoo Kang _____ (Signature)
(Co-Advisor)

¹ Declaration of Ethical Conduct in Research: I, as a graduate student of DGIST, hereby declare that I have not committed any acts that may damage the credibility of my research. These include, but are not limited to: falsification, thesis written by someone else, distortion of research findings or plagiarism. I affirm that my thesis contains honest conclusions based on my own careful research under the guidance of my thesis advisor.

Correlation Study of Surface Energy of Electrodes and Electrolytes with Lithium Ion Battery Performance

Hyejin Lee

Accepted in partial fulfillment of the requirements for the degree of
Master of Science

12.05. 2015

Head of Committee _____(인)

Prof. Hochun Lee

Committee Member _____(인)

Prof. Joongoo Kang

Committee Member _____(인)

Prof. Seung-Tae Hong

MS/ES
201424008

이혜진. Hyejin Lee. Correlation study of surface energy of electrodes and electrolytes with lithium ion battery performance. Department of Energy Systems Engineering. 2016
Advisors Prof. Hochun Lee, Co-Advisor Dr. Joongoo Kang.

ABSTRACT

Despite the huge success of the lithium-ion batteries (LIBs) in the portable electronic devices and electric vehicles (EVs) applications, the fundamental understanding on the electrode/electrolyte interface still remains challenging. The interfacial phenomena are governed by the physico-chemical properties of the electrode surface as well as the nature of electrolyte components.

At the first part of this work, the surface free energy (SFE) analysis is performed for various commercial grade LiMn_2O_4 (LMO) powders and the three SFE components, Lifshitz van der Waals (γ_s^{LW}), acid (γ_s^+), and base (γ_s^-), are obtained based on the van Oss-Chaudhary-Good (vOCG) theory. It is revealed that Mn dissolution is strongly correlated with the Lewis acid-base component ($\gamma_s^{\text{AB}} = 2\sqrt{\gamma_s^+ \cdot \gamma_s^-}$), which is attributed to the short-range columbic interactions between the Lewis acidic site of LMO surface (γ_s^+) and the basic electrolyte species (e.g., solvents, anions), and between the Lewis basic site (γ_s^-) and the acidic electrolyte species (e.g., HF).

At the second part, the SFE analysis is performed to shed some light on surface chemical properties of graphite anode and the solid-electrolyte interphase (SEI) layer formed on it. The edge and basal planes of pristine graphite show relatively high γ^+ and γ^- , respectively. The presence of SEI layer brings dramatic difference in the SFE properties of the graphite electrodes. In particular, the γ^- values becomes one order of magnitude higher. In addition, the SFE values also depend on the types of Li salt employed for SEI formation. LiPF_6 and LiFSI solutions form inorganic-rich SEI layer, and thus higher total SFE than the organic-rich SEI formed in a LiClO_4 solution.

At the last part, various polymers are examined to search a suitable probe solid triplet with a low condition number, which is mandatory to determine the three SFE components of liquid samples. Among the tested combinations, PE/PVF/PMMA set is found to have the lowest condition number, which is rather high compared to that of probe liquid set. Further exploration for better probe solid triplet is needed.

Keywords: LiMn_2O_4 , Surface free energy, metal dissolution, graphite electrode, SEI, condition number

Contents

Abstract	i
List of contents	ii
List of tables	iv
List of figures	v
I . Correlation of surface free energy and electrolyte property to assess metal dissolution behavior of LiMn_2O_4	
1.1 Introduction	1
1.1.1 Overview	1
1.1.2 Capillary rising method for porous materials	2
1.2 Experimental	3
1.2.1 Preparation of LMO electrodes	3
1.2.2 Metal dissolution	4
1.2.3 Activation energy of Mn dissolution reaction and Arrhenius equation	5
1.2.4 Adsorption method	7
1.3 Results and discussion	11
1.3.1 Analysis of the morphology of LiMn_2O_4	11
1.3.2 Contact angle measurement by sorption and surface energy	12
1.3.3 Effect of donor number on the Mn dissolution	16
1.3.4 Effect of HF content and Mn dissolution	19
1.3.5 Correlation between surface energy components and Mn dissolution ..	19
1.4 Conclusions	20
II . Surface energy analysis of pristine and SEI-formed graphite anodes	
2.1 Introduction	24
2.2 Experimental	24
2.2.1 Surface energy analysis of pristine graphite	29
2.2.2 SEI formation	31
2.3 Results	32

2.3.1 Surface energy analysis of graphite (edge and basal planes)	32
2.3.2 Surface energy analysis of SEI on the pyrolytic graphite	33
2.4 Conclusion and future plan	39
III. Solid surface energy analysis of polymers for solid probes	
3.1 Introduction	42
3.2 Experimental	48
3.3 Results	51
3.4 Discussion and future plan	54
References	56

List of tables

Table 1. SFE (γ_L) in (mJ/m²) of the probe liquids and their Lifshitz van der Waals forces (γ_L^{LW}), polar (γ_L^P), acid (γ_L^+) and base (γ_L^-) component. Surface energy components of HOPG, PGB, PGE.

Table 2. Properties of the electrolytes used for SEI formation in this study.

Table 3. Surface energy components of HOPG, PGB, and PGE.

Table 4. SFE components of the graphite electrode cycled in 1 M LiPF₆, LiClO₄, or LiFSI solution.

Table 5. Condition numbers by 3 liquid combination.

Table 6. Advancing angle data (first advancing angle/ second advancing angle).

Table 7. Advancing angle data that are reported from C. Della Volpe and Wu. (data from Wu).

Underlined data are one of closest measured value with the reported one.

Table 8. Solid surface energy by measuring advancing angle measurements.

Table 9. Screened solid triplets which has condition number less than 65.

List of figures

Figure 1. Schematic illustration of Mn dissolution mechanisms.

Figure 2. Schematic experimental setup for contact angle measurements at powders.

Figure 3. Procedure of Mn dissolution experiment to investigate the content of water and HF, and the concentration of dissolved Mn²⁺ ion in the electrolyte at various temperature storage (35 °C, 45 °C, 55 °C and 65 °C.).

Figure 4. Illustration of SFE interaction estimation by measuring contact angle measurement.

Figure 5. Fiber chamber SH0620 (Krüss, Hamburg, Germany).

Figure 6. Formamide adsorption mass change by time.

Figure 7. Adsorbed mass of probe liquids to filter.

Figure 8. SEM images of various LiMn₂O₄ powders.

Figure 9. Contact angle from adsorption method by using (a) water (b) diiodomethane (c) formamide for LMO samples.

Figure 10. Surface free energy components.

Figure 11. Mn dissolution of 1M LiPF₆ EC/EMC (1:2) after high temperature (60 °C) storage for 7 days.

Figure 12. Scheme of Gibbs free energy change during the Mn dissolution reaction; $3\text{Mn}^{3+} \rightarrow \text{Mn}^{4+} + \text{Mn}^{2+} + n \text{ (Solvent)}$, where n is the number of solvent.

Figure 13. Correlation between Mn dissolution in 1M LiPF₆ EC/EMC (1:2) solution and surface energy.

Figure 14. Correlations of Mn dissolution and donor number of electrolytes after high tempera-

ture (60 °C) storage for 7 days. .

Figure 15. Mn dissolution in THF, TMP, DMSO and EC with various HF content after high temperature (60 °C) storage for 7 days.

Figure 16. Schematic illustration of Mn dissolution. Polar SFE of electrode and electrolyte interact and drive the Mn dissolution.

Figure 17. (Left) Edge and Basal planes of graphite, (Right) commercial edge plane graphite electrode used in this study.

Figure 18. The depth profile of the SEI formed on the basal plane (left) and edge plane (right) of HOPG.

Figure 19. Estimated composition of the SEI on HOPG in electrolyte.

Figure 20. Reductive decompositions of electrolyte salts on carbonaceous anodes.

Figure 21. Surface energy components (a) Total, (b) Basicity and (c) Acidity of PGE, PGB and HOPG electrode.

Figure 22. CVs for SEI formation in 1M (a) LiPF₆ (b) LiFSI and (c) LiClO₄ in EC/DEC (1/2, v/v). Data form edge planes (left) and basal planes (right).

Figure 23. Surface energy components total, basicity and acidity of PGE and PGB electrodes with 1M LiPF₆, LiClO₄ and LIFSI salt

Figure 24. High condition number (left) and low condition number triplet (right) for solid surface energy measurements.

Figure 25. Polymer sample preparing for contact angle measurement.

Figure 26. Schematic view of advancing angle measurement.

Figure 27. Typical advancing angle measurement time-contact angle graph. This data is from water contact angle on PE film.

I . Correlation of Surface free energy and electrolyte property to assess metal dissolution behavior of LiMn_2O_4

1.1. Introduction

1.1.1 Overview

Lithium ion batteries (LIBs) have attracted much attention because of its potentials for portable devices and electric vehicles (EVs). Despite vast amount of efforts so far, understanding an interfacial phenomenon between electrolyte and electrodes still remains challenging. In the case of LiMn_2O_4 (LMO) cathode material, Mn dissolution issue is known to be the key failure cause. The Mn dissolution behavior, a cathode/electrolyte interfacial phenomenon, is expected to be determined by the physico-chemical properties of the cathode surface as well as the nature of electrolyte components. However, the correlation between the chemical properties of cathode surface and the metal dissolution behavior is not fully understood yet.

In this work, a surface free energy (SFE) analysis is employed to verify surface chemical properties of LMO powders with an aim to assess the Mn dissolution behavior.

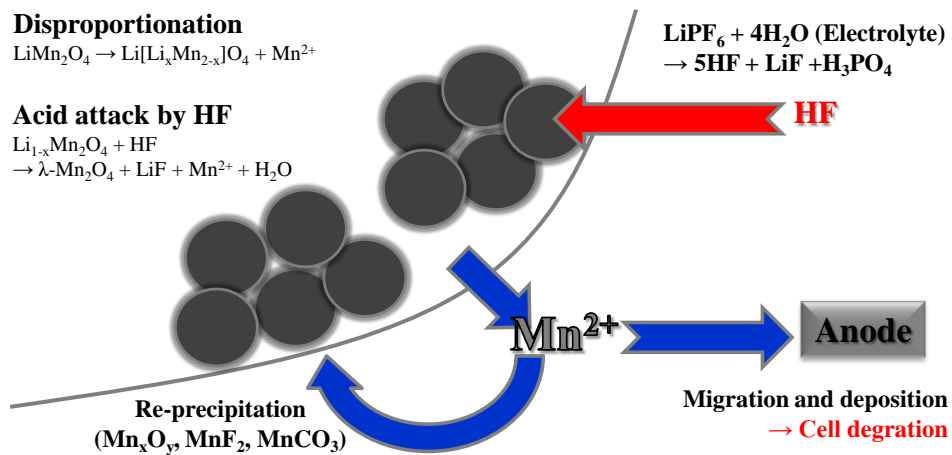


Figure 1. Schematic illustration of Mn dissolution mechanisms.

1.1.2 Capillary rising method for porous materials

Contact angles of porous powders can be measured by capillary rising method. According to Washburn, we can calculate the contact angle of porous powder by measuring adsorbed liquid height by times.

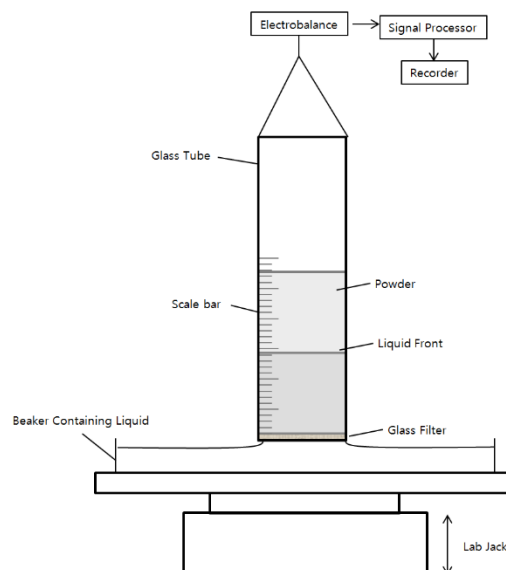


Figure 2. Schematic experimental setup for contact angle measurements at powders [1].

Relations of capillary rising can be described by Washburn equation [2].

$$\frac{dh}{dt} = \frac{r^2}{8\eta h} \left(\frac{2\gamma_{lv}\cos\theta}{r} - \Delta\rho gh \right) \quad (\text{Eq. 14})$$

, where h is the height of liquid penetration at time t, r is the radius of capillary. γ_{lv} is the liquid to vapor surface tension, θ is the contact angle, $\Delta\rho$ is the difference in density between the liquid and the gas phase, and η is the viscosity. Washburn equation can be measured by detection of m^2/t and can be simplified by measuring capillary constant. Capillary constant can be obtained by measuring m^2/t with totally wetting liquid which is n-hexane.

$$\cos\theta = \frac{m^2}{t} \times \frac{\eta}{\rho^2\sigma_L c} \quad (\text{Eq. 15})$$

$$c = \frac{1}{2} \pi^2 r^5 n_k^2 \quad (\text{Eq. 16})$$

,where r is radius of the micro capillaries between powder particles, n_k is the number of powder particles. Capillary rising method cannot be used for above 90°: no liquid can penetrate to the powder above 90° [1-4].

1.2. Experimental

1.2.1 Preparation of LMO electrodes

Cathode slurry was prepared by combining LMO powder (L&F Co., Korea) as active mate-

rial, Super-P as conductive carbon and PVdF (KF 9130, Kureha) as binder. NMP was used as solvent to adjust the viscosity of the slurry. The four ball-milled slurries were uniformly coated onto Al foil which is current collector and dried in oven at 110 °C for 30 min. The dried electrodes were pressed and then dried again in a vacuum oven at 80 °C overnight. The electrodes were cut into pieces of diameter 14mm, with $8.45 \pm 0.1 \text{ mg/cm}^2$.

1.2.2 Metal dissolution

To investigate the influence of the surface free energy (SFE) on the metal dissolution behavior, one piece of the LMO electrode (14 mm diameter) was stored with 4ml of electrolyte in a polytetrafluoroethylene (PTFE) bottle (Cowie) at 60 °C for 7 days. The electrolyte which is composed of 1M LiPF_6 in EC/EMC (3/7 by volume, LG chem.) is used. The water contamination in the electrolyte is under 10 ppm, and the electrolyte is stored in glove box which is filled with Argon gas. After the high temperature (60 °C) storage with LMO electrode, the concentration of metal ion in the electrolyte was analyzed by using atomic absorption spectroscopy (AAS, Shimadzu). At the same time, contents of water and HF were analyzed by Karl Fisher (831 KF coulometer, Metrohm) and acid-base titration methods (848 Titrino plus,

Metrohm).

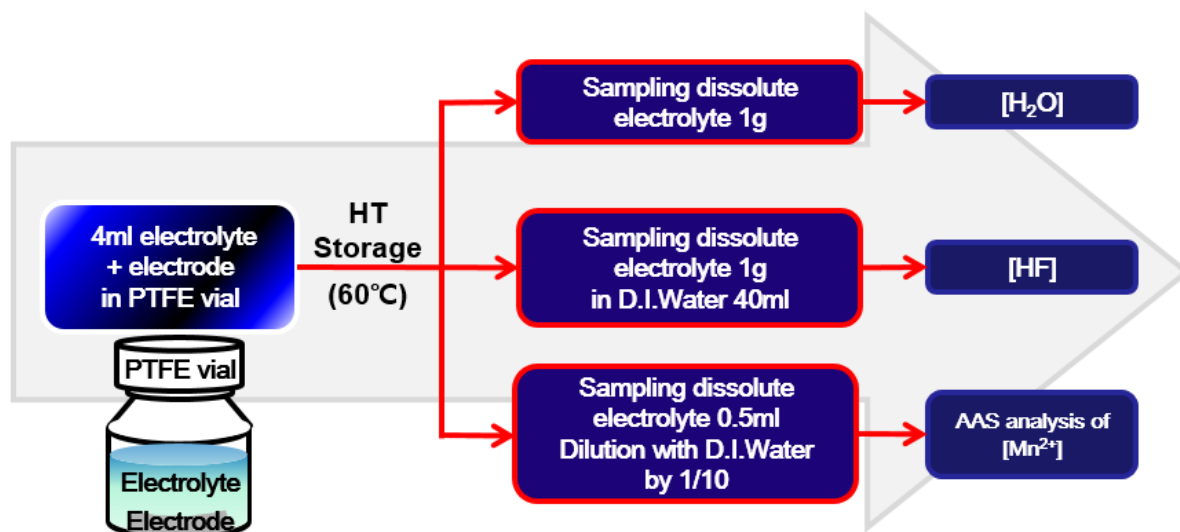


Figure 3. Procedure of Mn dissolution experiment to investigate the content of water and HF, and the concentration of dissolved Mn²⁺ ion in the electrolyte at various temperature storage (35 °C, 45 °C, 55 °C and 65 °C).

1.2.3 Activation energy of metal dissolution reaction and Arrhenius equation

All molecules possess a certain minimum amount of energy. The energy can be in the form of kinetic energy or potential energy. When molecules collide, the kinetic energy of the molecules can be used to stretch, bend, and ultimately break bonds, leading to chemical reactions. If molecules move too slowly with little kinetic energy, or collide with improper orientation, they do not react and simply bounce off each other. However, if the molecules are

moving fast enough with a proper collision orientation, such that the kinetic energy upon collision is greater than the minimum energy barrier, then a reaction occurs. The minimum energy requirement that must be met for a chemical reaction to occur is called the activation energy, E_a . In this study, E_a is separated into two part, adhesion related activation energy and non-related energy.

$$E_a = W_{adh} + E_a' \quad (\text{Eq. 17})$$

, where W_{adh} is work of adhesion and E_a' is adhesion non-related activation energy. Adhesion related activation energy can be expressed like following equation, as described before.

$$W_{adh} = \sqrt{(\gamma_S^{LW} \cdot \gamma_I^{LW})} + \sqrt{(\gamma_S^+ \cdot \gamma_I^-)} + \sqrt{(\gamma_S^- \cdot \gamma_I^+)} \quad (\text{Eq. 18})$$

SFE components are responsible for interacting forces, and Figure 5. reflected this idea.

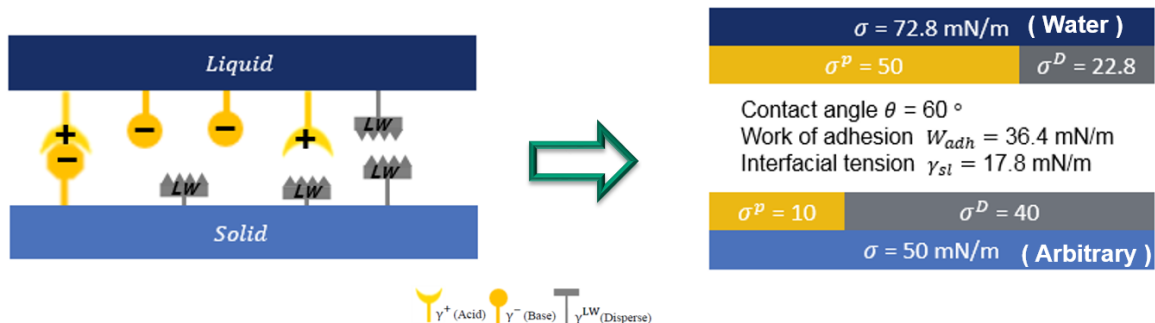


Figure 4. Illustracion of SFE interaction estimation by measuring contact angle measurement.

The fraction of molecules with energy equal to or greater than E_a is given by the exponential term in the Arrhenius equation:

$$k = A \exp\left(-\frac{E_a}{RT}\right) \quad (\text{Eq. 19})$$

$$\ln(k) = \ln(A) - \frac{E_a}{RT} \quad (\text{Eq. 20})$$

k is the rate constant, E_a is the activation energy, R is the gas constant, T is temperature in Kelvin, and A is frequency factor constant or also known as pre-exponential factor or Arrhenius factor. It indicates the rate of collision and the fraction of collisions with the proper orientation for the reaction to occur.

Combining 2 equation (18) and (20), we can deduce the relationship between reaction rate and acid-base components.

$$\ln(k; \text{Rate}) \propto \sqrt{(\gamma_S^{\text{LW}} \cdot \gamma_I^{\text{LW}})} + \sqrt{(\gamma_S^+ \cdot \gamma_I^-)} + \sqrt{(\gamma_S^- \cdot \gamma_I^+)} \quad (\text{Eq. 21})$$

1.2.4 Adsorption method

The adsorption method (capillary rise technique) was used to measure the contact angles of the cathode powders for the Li-ion batteries. Tensiometer K100 (Krüss, Hamburg, Germany) was used for contact angle measurement of cathode powders filled in SH0620 fiber chambers

as showed in the Fig. 5.



Figure 5. Fiber chamber SH0620 (Krüss, Hamburg, Germany).

All powder samples were also stored in a 110°C vacuum furnace for over one day before measurement to dehydrate. The properties of the cathode powders were changed according to the time exposed to air due to the humidity. Therefore the contact angles were measured within one hour. Capillary constant must be measured to determine the contact angles of porous materials such as cathode powder for Li-ion batteries. The n-hexane was used to measure capillary constant which has only dispersity part, not any of polar part. So the capillary constant was calculated by using Washburn's equation due to the fact that the contact angle should be zero. So the $\cos\theta$ was equal to one. The other terms are constant so, we can calcu-

late the capillary constant.

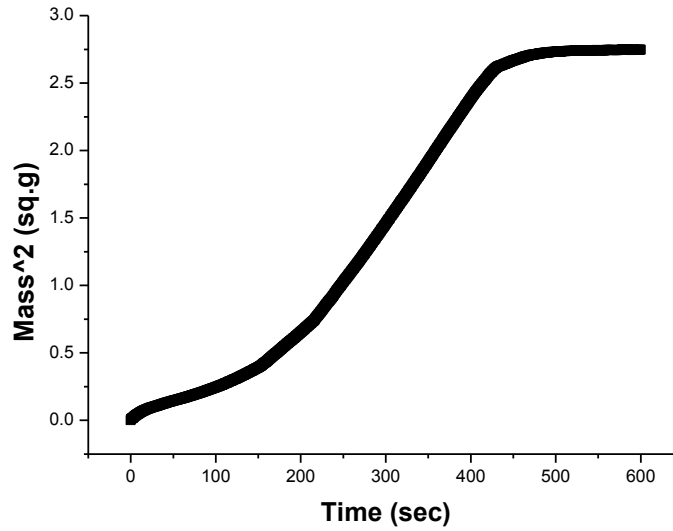


Figure 6. Formamide adsorption mass change by time.

After that, by measuring mass changes by the adsorption of known probe liquids by time, the contact angles of powder cathode by each probe liquids were calculated by using Washburn equation (Eq. 3). The mass square changes by time were chosen of its maximum gradient after the filter noises. Fig. 6 showed a square of absorbed liquid mass by the time.

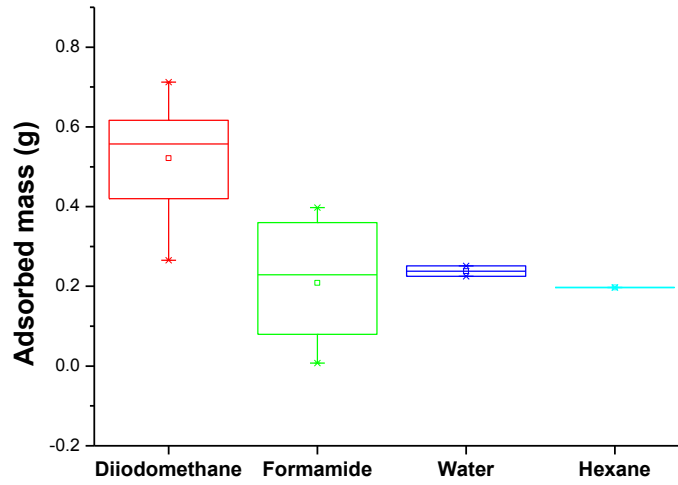


Figure 7. Adsorbed mass of probe liquids to filter.

Fig. 7. showed the adsorbed mass of probe liquids to filter. Diiodomethane adsorbed more and rapidly to the powder cathode than other probe liquids. So diiodomethane needed more cautious to loading the powder. To calculate SFEs of porous material the van Oss-Chaudhury-Good (vOCG) equation was used.

$$\cos \theta = \frac{m^2}{t} \times \frac{\eta}{\rho^2 \sigma_{LC}} \quad (\text{Eq. 22})$$

1.3 Results and discussion

1.3.1 Analysis of the morphology of LiMn_2O_4

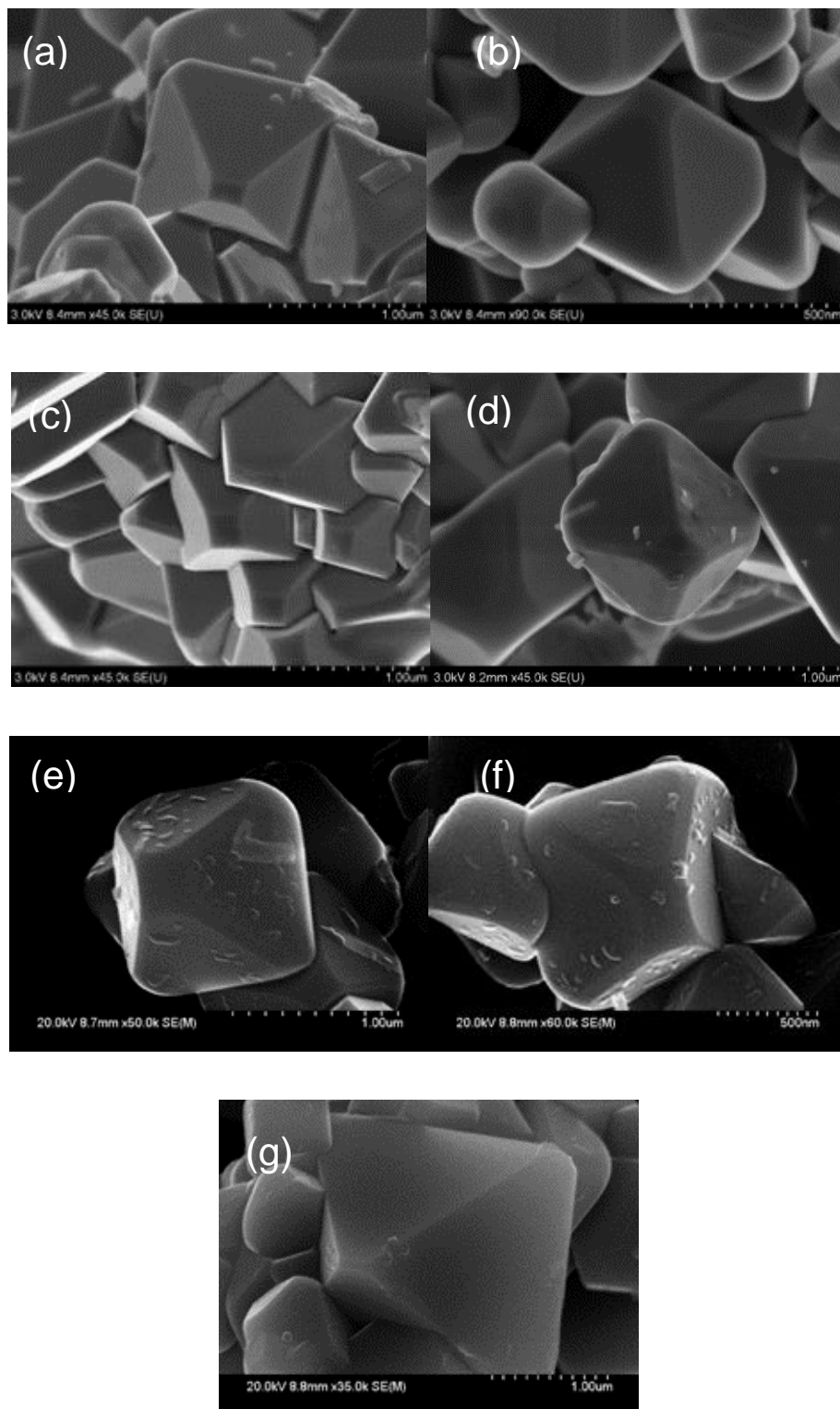
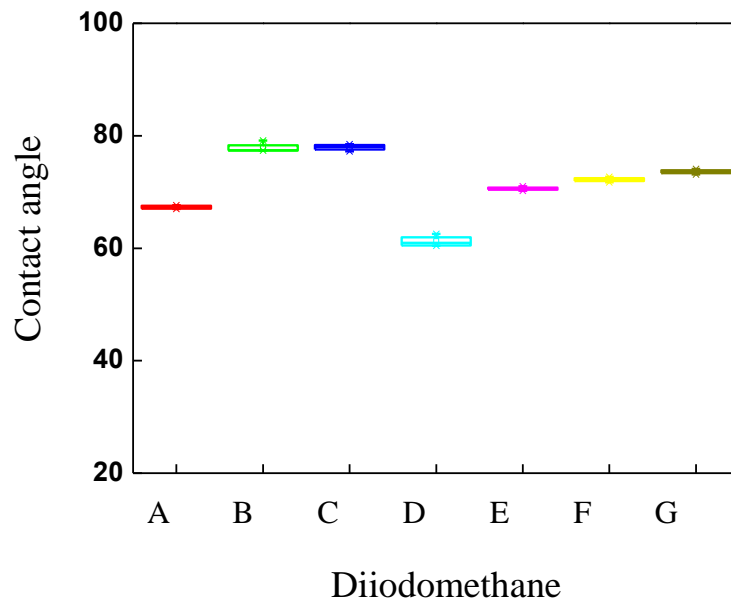
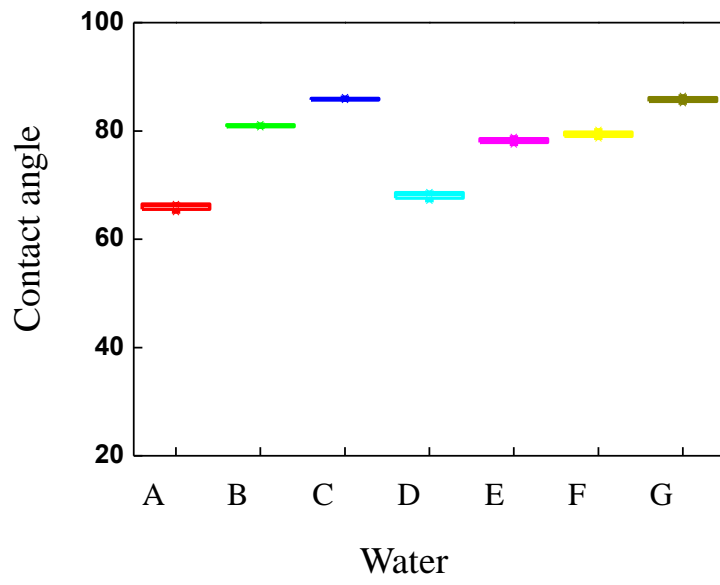


Figure 8. SEM images of various LiMn_2O_4 powders.

Morphologies of LiMn_2O_4 powders were investigated using SEM. Seven materials have some difference of shapes according to synthesis processes. Particle features may differ a Mn dissolution behavior since exposed termination plane has different cleavage energy which is a measure of the relative stability of different surface orientations and terminations. In other words, stability of each exposed plane affects the Mn dissolution phenomenon.

1.3.2 Contact angle measurement by sorption and surface energy

Contact angle of each powders and liquids are measured by utilizing Washburn equation and sorption method. Few times of experiments were carried out to get a reliable data, and, for each liquid-solid set, boxes are sketched in the range from 25% to 75%. The collected data sets are plotted on the graph below, and mean values were employed to analyze the surface energy of materials.



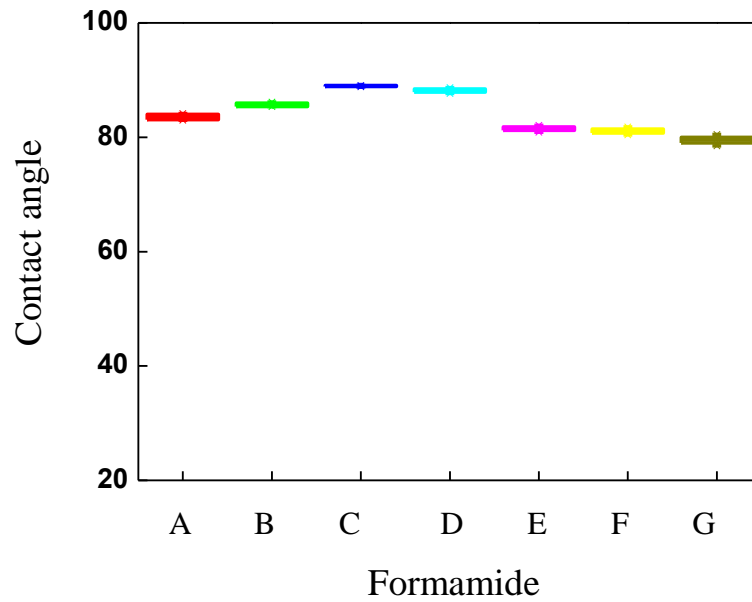


Figure 9. Contact angle from adsorption method by using (a) water (b) diiodomethane (c) formamide for LMO samples.

By utilizing three contact angle and vOCG theory, we can calculate acid-base component of solid. Fig 10. shows various surface free energy components which is total, dispersity, polarity, acid and base. In general, surface free energy of dispersity showed higher than polarity. It is attributed by a problem of water reference in vOCG scale. Also surface free energy of total, polar and acid components showed same trend. On the contrary, the other showed different trend.

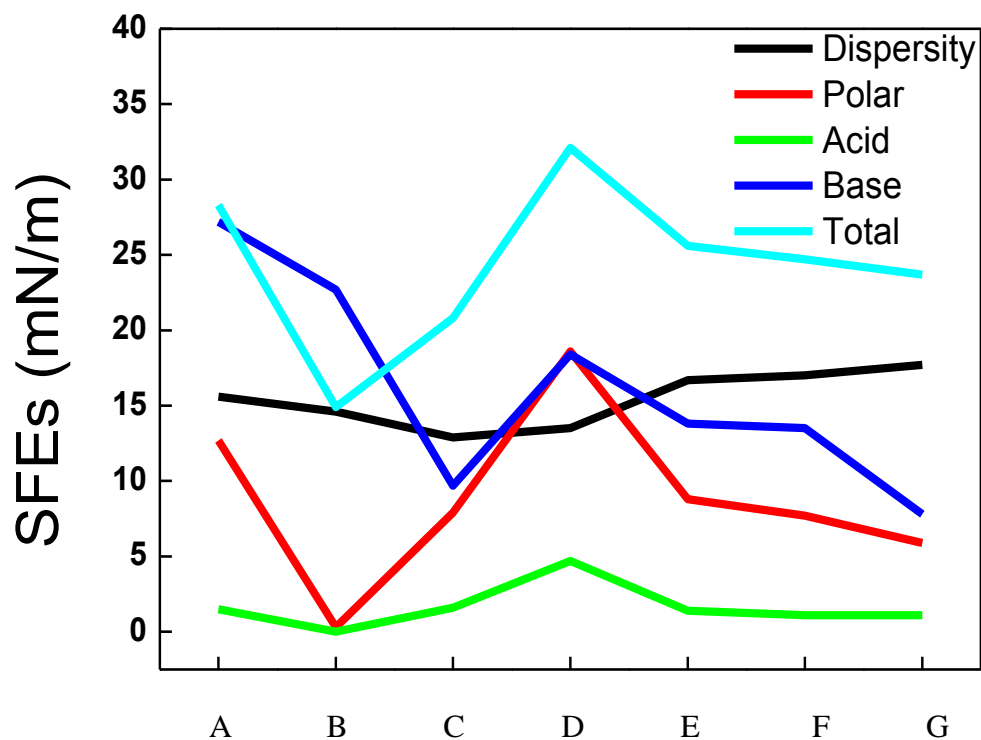


Figure 10. Surface free energy components.

To investigate the correlation of the surface free energy of LMO materials with metal dissolution, we conducted an experiment at high temperature (60°C) for 7days. Fig 8. shows metal dissolution of various LMO electrodes measured by an atomic absorption spectroscopy.

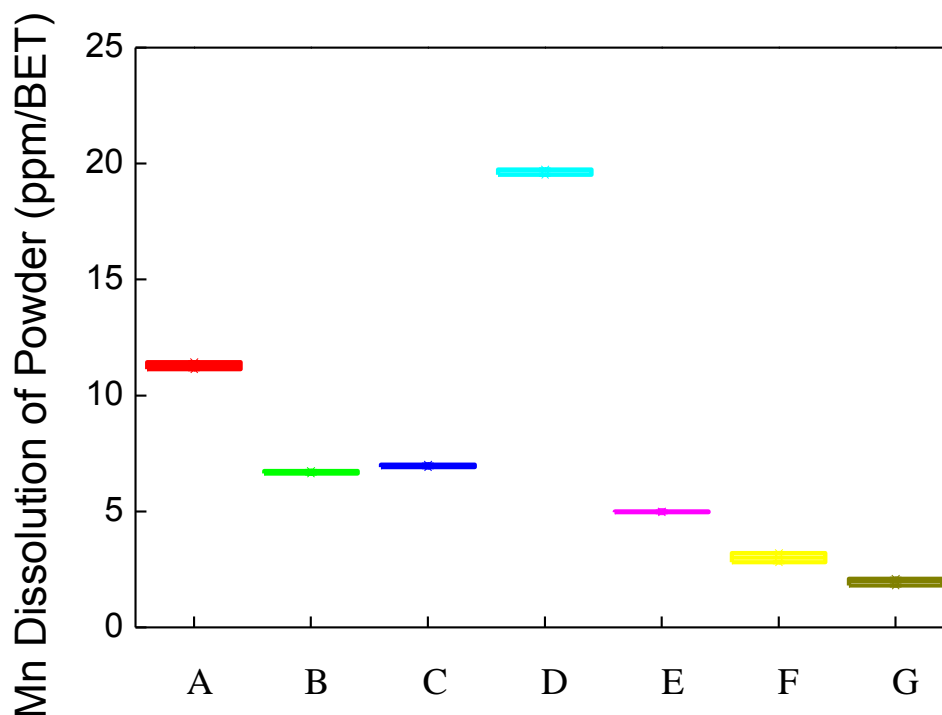


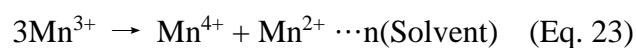
Figure 11. Mn dissolution of 1M LiPF₆ EC/EMC (1:2) after high temperature (60 °C) storage for 7 days.

1.3.3 Correlation between surface energy components and Mn dissolution

To understand the result of increasing Mn dissolution in order of solvent's donor number and HF content, it was approached from a theoretical point of view. When Mn dissolution reaction occurs, disproportionation of manganese and solvation of Mn²⁺ with the solvent can be formularized as Eq.23, where n is the number of solvated solvent, S is solvent molecule.

From Eq.1, kinetics of Mn dissolution is represented as Eq. 24. According to the Arrhenius'

equation, the reaction rate is exponentially proportional to the Gibbs free energy of dissolution as Eq.25, and this Gibbs free energy means solvation energy. Considering donor number represents solvation energy, the experimental result that the rate of Mn dissolution is exponentially proportional to the donor number of the solvent can be demonstrated.



$$k = \frac{[\text{Mn}^{4+}][\text{Mn}^{2+}]}{[\text{Mn}^{3+}]^2} \quad (\text{Eq. 24})$$

$$k = A e^{-E_a/RT} \quad (\text{Eq. 25})$$

In other words, when two different solvent have different solvation energy, for example, solvent 2 has higher solvation energy than solvent 1, the activation energy of solvent 2 is lower than solvent 1, with the relationship between solvation energy and activation energy.

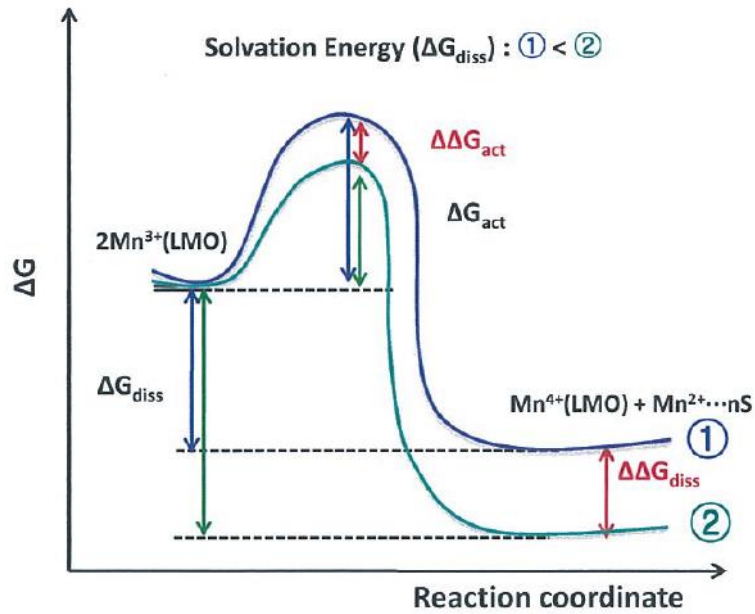


Figure 12. Scheme of Gibbs free energy change during the Mn dissolution reaction: $3\text{Mn}^{3+} \rightarrow \text{Mn}^{4+} + \text{Mn}^{2+} \cdots n\text{(Solvent)}$, where n is the number of solvent.

Remind an equation below that work of adhesion is proportional to the acidity and basicity of each solid and liquid and activation energy of Mn dissolution.

$$\ln(k; \text{Rate}) \propto \sqrt{(\gamma_S^{\text{LW}} \cdot \gamma_I^{\text{LW}})} + \sqrt{(\gamma_S^+ \cdot \gamma_I^-)} + \sqrt{(\gamma_S^- \cdot \gamma_I^+)} \quad (\text{Eq. 26})$$

According to the above equation, we conclude that acid site interacts with electrode donating property of electrolyte (donor number), and base site reacts with H^+ ions (electron accepting property of electrolyte) with a root scale. To verify this hypothesis, dissolve Mn amount of 7 different LMO and its acidity, basicity were plotted below. Long range interaction seems not affect to the metal dissolution, but other acidity and basicity of solid had a lin-

ear dependency with Mn dissolution.

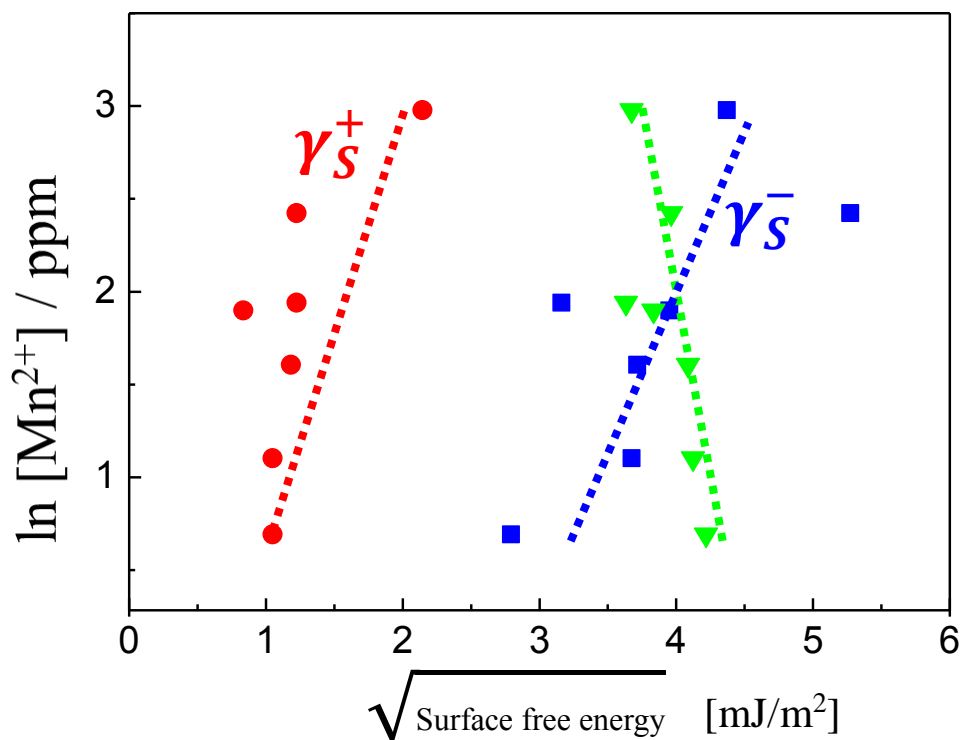


Figure 13. Correlation between Mn dissolution in 1M LiPF₆ EC/EMC (1:2) solution and surface energy.

1.3.4 Effect of donor number on the Mn dissolution

Mn dissolution experiment with other solvents instead of EC was performed. Other solvents are fluoroethylene carbonate (FEC), propyl carbonate (PC), ethyl acetate (EA), butyronitrile (BN), tetrahydrofuran (THF), 1,2-dimethoxyethane (1G), Trimethyl phosphate (TMP), 1-methyl-2-pyrrolidinone (NMP) and dimethyl sulfoxide (DMSO). 1M LiPF₆ X/EMC (1/2 by

volume, X=FEC, PC, EA, BN, THF, 1G, TMP, NMP or DMSO) were stored at 60°C oven for 7 days with a piece of LMO electrode. As shown in Fig. , the Mn dissolution is exponentially proportional to the donor number (DN) of solvents. The DN is a quantitative measure of basicity in chemistry. In other words, donor number reflects the electron donating property (basicity of electrolyte).

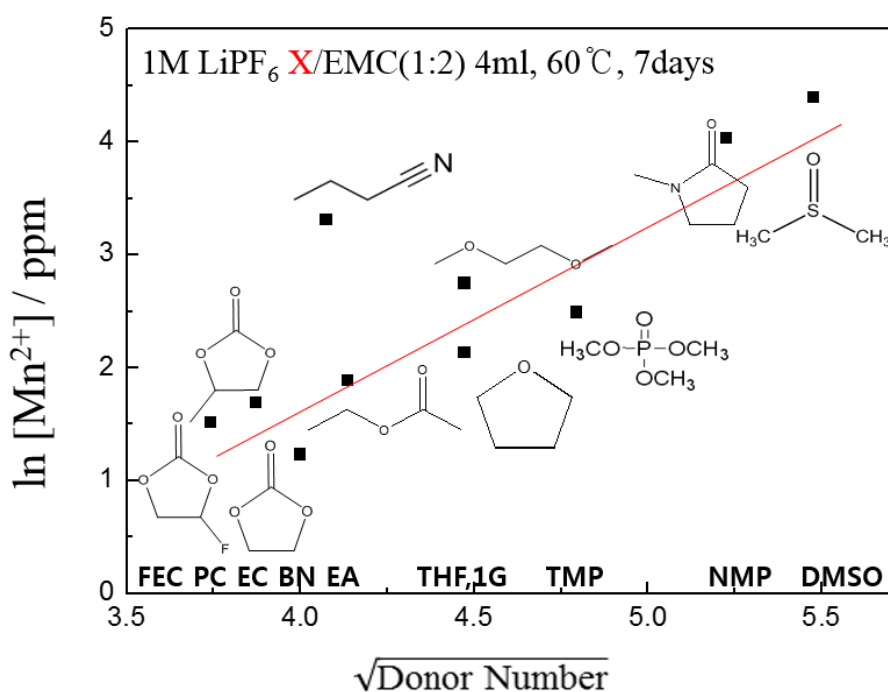


Figure 14. Correlations of Mn dissolution and donor number of electrolytes after high temperature (60 °C) storage for 7 days.

1.3.5 Effect of HF content and Mn dissolution

Mn dissolution experiment with various HF contents (0, 50 100, 200 ppm) were used in

this study. Solvents are ethyl methyl carbonate (EMC), ethyl carbonate (EC), 1,2-dimethoxyethane (1G), trimethyl phosphate (TMP), and dimethyl sulfoxide (DMSO). 1 M LiPF₆ X/EMC (1:1 by mol, X=EMC, EC, 1G, TMP or DMSO) were stored at 60 °C oven for 7 days with a piece of LMO electrode. Mn dissolution is exponentially proportional to the HF content. It may led to the conclusion that HF, which can be electron accepting property of electrolyte, causes the Mn dissolution.

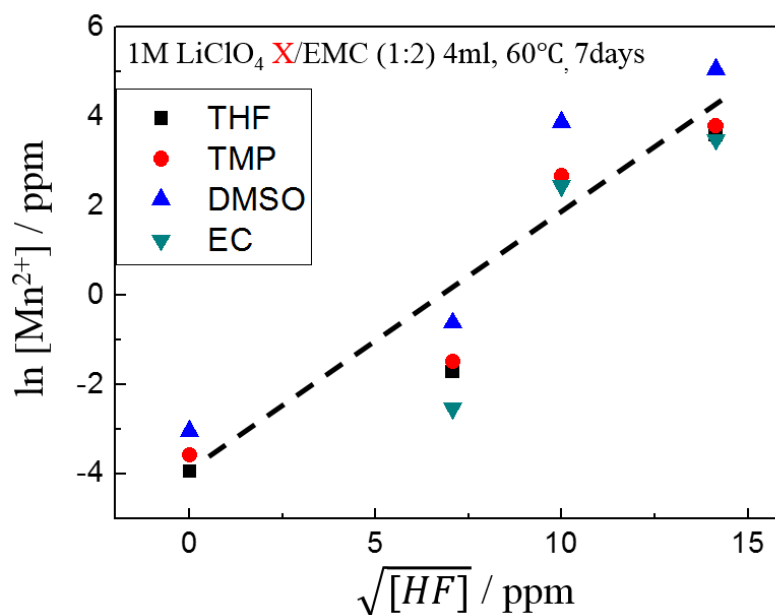


Figure 15. Mn dissolution in THF, TMP, DMSO and EC with various HF content after high temperature (60 °C) storage for 7 days.

2.4. Conclusions

The SFE and Mn dissolution property of various LMO was determined by sorption method in this work. Polar SFE implies a surface acid or base functionality. For this reason, it was possible to infer the correlation between Mn dissolution behavior and SFE. The γ^+ and γ^- of solid, were proportional to the Mn dissolution. Although the SFE components of the electrolyte have not been determined yet, HF concentration and donor number of the electrolyte were assumed to represent the γ^+ and γ^- of the electrolyte. Donor number is a quantitative measure of basicity in chemistry. When the solvent has higher donor number, it showed the proportional relationship with Mn dissolution. Also, HF content played a γ^+ role of electrolyte, so when H⁺ ions increases, it led to more Mn dissolution. This data provides a possible explanation that actual electron donating property (donor number) and HF content (electron acceptor) can be electrolyte acid and base characteristic. This work was the first correlation work between SFE and battery performance, also suggests the practical use of SFE analysis to predict the battery performance.

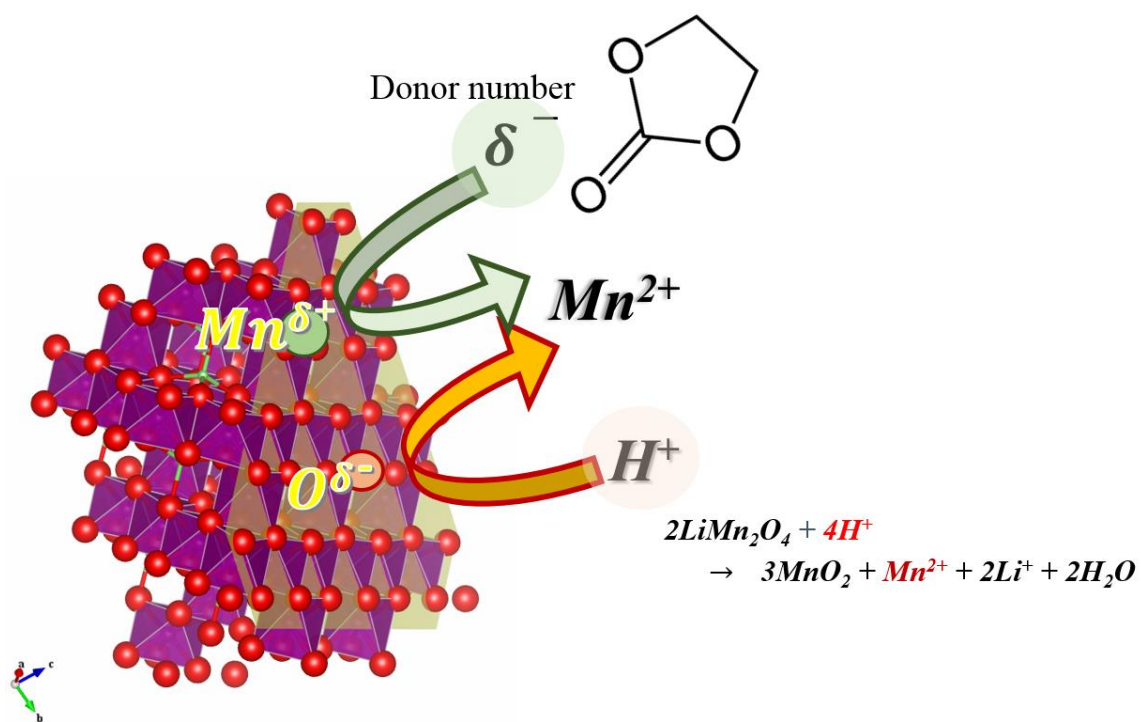
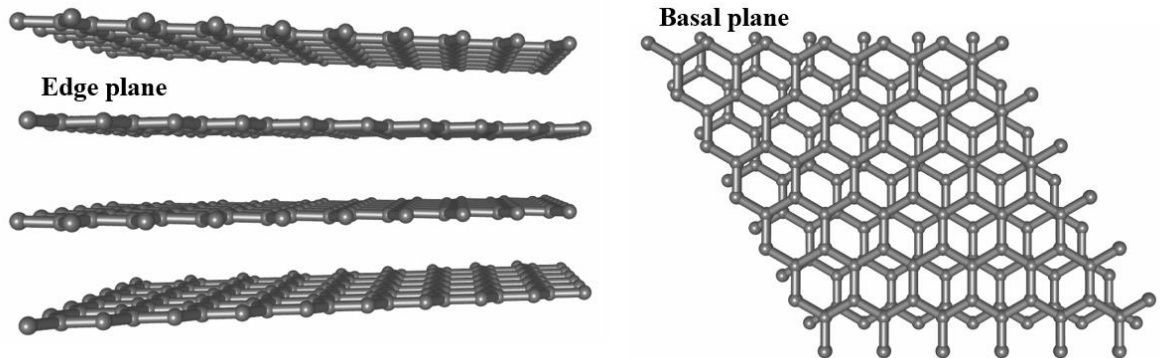


Figure 16. Schematic illustration of Mn dissolution. Polar SFE of electrode and electrolyte interact and drive the Mn dissolution.

II. Surface energy analysis of pristine and SEI-formed graphite anodes

2.1 Introduction

Graphite has long been employed as an anode material for the lithium-ion batteries (LIBs) due to its high capacity and good cyclability. It is well known that the electrochemical performances of a graphite anode heavily depends on the solid electrolyte interphase (SEI) layer, which is formed on the anode surface as a result of electrolyte decomposition at the first charge (Li-intercalation) process.





**Commercial Graphite
(Edge & Basal) Electrodes**

Figure 17. (Upper) Edge and Basal planes of graphite, (bottom) commercial edge plane graphite electrode used in this study.

The reactivity of carbon atoms at the edge sites is much higher than that of carbon atoms in the basal planes [5,6]. As seen in Fig. 1. graphite has edge and basal plane depending on exposed facet. Consequently, the physical and chemical properties of carbon vary with basal-edge plane ratio. The role of the SEI on the different planes of graphite particles is different: on the basal plane, it is sufficient to have an electronic non-conducting film; on the cross section (edge planes) it must also be a good lithium ion conductor. This difference can be reflected in a composition difference. Therefore it is important to study separately the composition and properties of the SEI on these two planes (basal and cross section) [7]. In this study, commercial graphite electrodes (In Figure 18) were used to body out the edge and basal systems.

So far, extensive efforts have been devoted to elucidate the structure, chemical composition, ion transport behavior and failure mechanism of the SEI layer. The physicochemical properties of the graphite surface are naturally expected to determine the characteristics of an SEI layer because the SEI formation is the electrochemical reaction taking place at the graphite/electrolyte interface. Fig. 1. presents the change in atomic concentration of the elements found as a function of sputtering time. Some material decomposition and surface chemical reactions are to be expected. These factors may affect the concentration depth profile, but does not change it drastically in the basal plane. For the edge plane case, the carbon signal decreases sharply after sputtering. This is accompanied by drop in the oxygen atomic concentration, and this may indicate that organic compound, like polyolefin and polymers containing oxygen, are presented only on SEI surface close to the electrolyte.

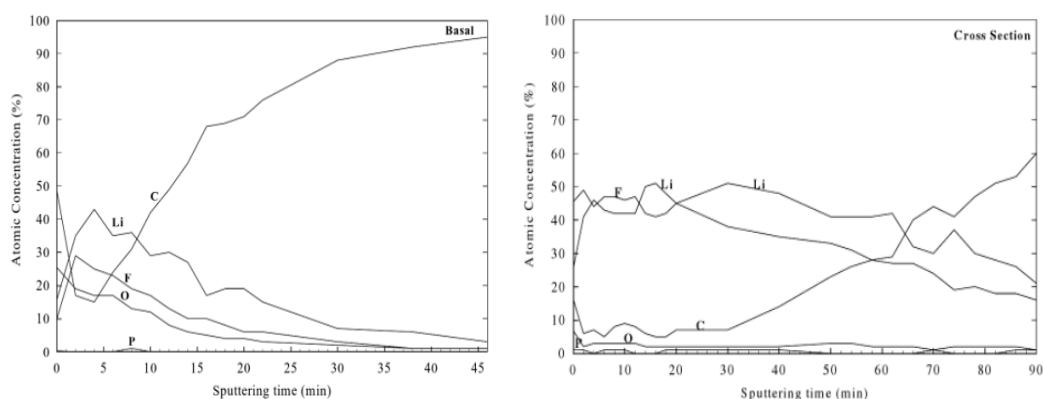


Figure 18. The depth profile of the SEI formed on the basal plane (left) and edge plane (right) of HOPG [8].

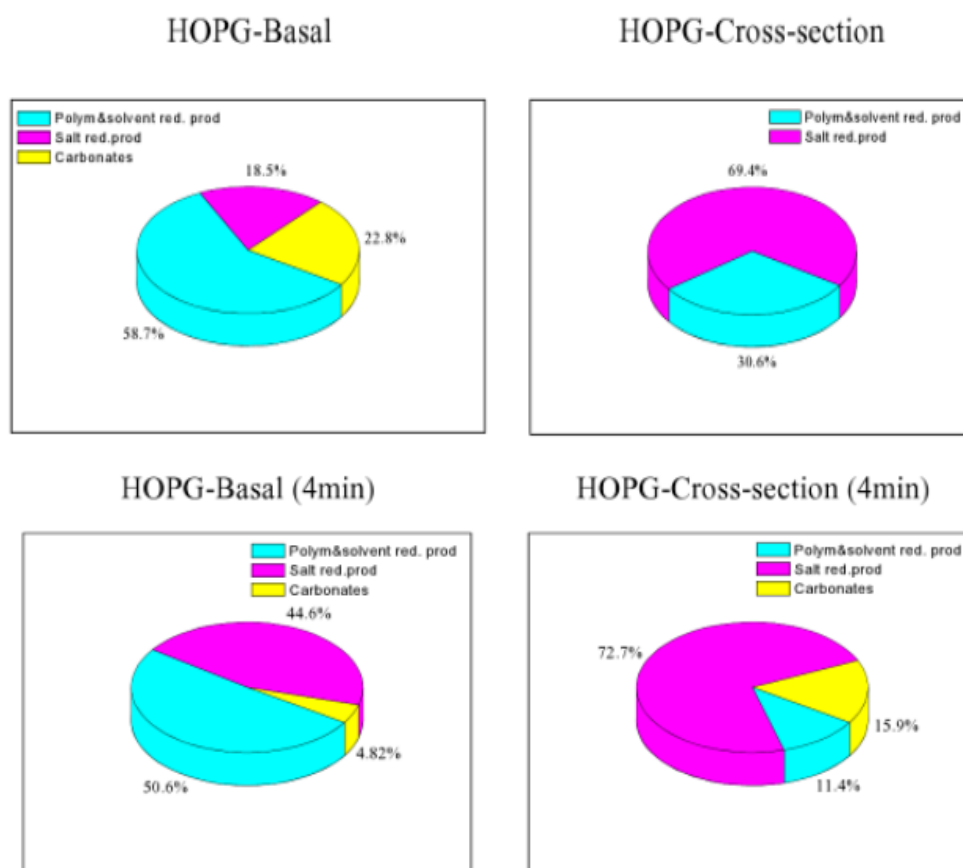


Figure 19. Estimated composition of the SEI on HOPG in electrolyte [8].

On the basis of the data in Figure 20, it is suggested that graphite has a more pronounced influence on SEI formation. Although much work has been done about SEI film, the

effects of the surface properties of graphite anode on the growth reaction and the nature of SEI layer are not fully understood yet.

When electrolyte solution begins to reduce on the graphite surface and forms SEI, there are competing and parallel solvent and salt reduction processes. Salt degradation products and organic compounds that are reduction products of the solvent made up of the SEI. For this reason, SFE of SEI with differing salt can be interesting topic of this study.

Salt	
	LiClO ₄ : $\text{LiClO}_4 + ne + 2n \text{Li}^+ \rightleftharpoons \text{Li}_2\text{O} + \text{LiClO}_3, \text{LiClO}_2 + \text{LiCl}$
	LiAsF ₆ : $\text{LiAsF}_6 + 2e + 2 \text{Li}^+ \longrightarrow \text{AsF}_3 + 3\text{LiF}$ $\text{AsF}_3 + 2ne + 2 n\text{Li}^+ \longrightarrow \text{Li}_n\text{AsF}_{3-n} + n\text{Li}^+$
	LiPF ₆ : $\text{LiPF}_6 + 2e + 2\text{Li} \longrightarrow \text{PF}_3 + 3\text{LiF}$ $\text{LiPF}_6 \rightleftharpoons \text{LiF} + \text{PF}_5$ $\text{PF}_5 + \text{H}_2\text{O} \longrightarrow 2\text{HF} + \text{POF}_3$ $\text{PF}_5 + 2ne + 2 n \text{Li}^+ \longrightarrow \text{LiPF}_{6-n} + n\text{LiF}$

Figure 20. Reductive decompositions of electrolyte salts on carbonaceous anodes [9]

A prior study has suggested that the active surface area (ASA) of graphite represents the edge plane reactivity toward electrolyte: if ASA is high enough ($\geq 0.1 \text{ m}^2/\text{g}$), an efficient SEI can be formed and the graphite exfoliation is prevented [10]. It was also claimed that the irreversible capacity at the first cycle is proportional to ASA, the specific surface area, and the amount of oxygenated surface groups [11].

When it comes to the cathode case, surface active area may cause electrolyte separa-

tion. Typical cathodes, such as LiCoO_2 and LiMn_2O_4 , have polarity on their surface. This polarity preferentially adsorbs the cyclic carbonates than linear carbonates because cyclic carbonates have higher dielectric constant. More polarized species can be more easily affected by an acid- base interaction of electrode and electrolyte. It would be reasonable to assume that the binding strength between the electrode polar surface and EC or PC is much stronger than the less-polar linear carbonates, like DMC and DEC. Preferential adsorption on the cathode surface has also revealed with a spectroscopic analysis using the sum frequency generation (SFG) [12].

In this study, the surface free energies (SFEs) of pristine and SEI-formed graphite anodes are examined. First, the SFE properties of the edge and basal planes of graphite are examined. Second, the SFE characteristics of the SEI layers formed on the edge/basal planes in various Li- salt electrolytes are investigated.

2.2 Experimental

2.2.1. Surface energy analysis of pristine graphite

The contact angle measurements were carried out using three probe liquids; ultra-pure wa-

ter (W), formamide (F), diiodomethane (D). The values of SFE of the probe liquids and its components, used for the calculations, are presented in the Table 7. The contact angles (CA) were measured by the sessile drop method using a DSA100 goniometer (Krüss, Germany) at room temperature. SFE was derived based on van-Oss-Chaudhury-Good (vOCG) theory [13].

Table 1. SFE (γ_L) in (mJ/m²) of the probe liquids and their Lifshitz van der Waals forces (γ_L^{LW}), polar (γ_L^P), acid (γ_L^+) and base (γ_L^-) component.

Liquid	γ	γ^{LW}	γ^{AB}	γ^+	γ^-
Water (W)	72.8	21.8	51	25.5	25.5
Formamide (F)	58	39	19	2.28	39.6
Diiodomethane (D)	50.8	50.8	0	0	0

HOPG (highly ordered pyrolytic graphite, 10x10x1.6 mm, Alfa aser) and PGB (pyrolytic graphite-basal plane, area = 0.70 cm², ALS/Japan) were used to represent the basal plane, and PGE (pyrolytic graphite-edge plane, area = 0.70 cm², ALS/Japan) represented the edge plane of the graphite, respectively. Electrodes were polished on emery paper (#3000, 7 μ m grit size) and alumina (0.3 μ m diameter) slurry on a polishing pad. After the mechanical polishing, graphite materials were rinsed with distilled water in the ultrasound bath for 30 s to

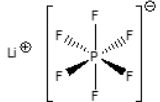
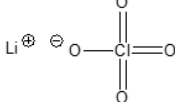
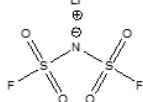
avoid any possible contamination by emery paper or alumina powder.

2.2.2 SEI formation

A standard three-electrode configuration in a flooded cell (polyethylene round bottle, 22 mm diameter) with 4 ml electrolyte was employed for the SEI formation. Li and Pt wire served as reference and counter electrode, respectively. The pyrolytic graphite electrode (area = 0.07 cm²) from ALS (Japan) was used as a working electrode. Cyclic voltammetry (CV) was performed over 3.5 – 0.005 V at scan rate 5 mV s⁻¹ in Ar filled glove box. This CVs of graphite electrodes in 1 M LiFSI, LiClO₄, and LiPF₆ in EC/DEC (1/2, v/v) solutions are plotted in Fig.

3. Different characteristics of mentioned solutions were also given in Table 8.

Table 2. Properties of the electrolytes used for SEI formation in this study.

EC/DEC (1/2, v/v)	1M LiPF ₆	1M LiClO ₄	1M LiFSI
Chemical structure			
Conductivity [mS/cm]	7.68	5.06	8.84
Viscosity [m Pa s]	4.55	4.22	1.23
SFE [mN/m]	29.37	28.05	29.96

2.3. Results

2.3.1 SFE analysis of pristine edge and basal graphite

The measured SFE values of graphite electrodes are given in Table 1, and compared in Fig. 5. HOPG and PGB exhibit similar total SFE around 40–45 mN/m², and PGE shows higher total SFE over 50 mN/m².

Two basal plane graphites, PGB and HOPG, show similar SFE behavior. It is generally known that basal plane of graphite has abundant electrons, consisting of π -conjugated sp² carbon atoms, which seems to be responsible for the strong basicity (γ^-) of basal plane. In contrast, edge plane exhibits higher γ^+ value. The electron transfer rate is 7 orders of magnitude higher at the edge plane than at its basal plane. The high electron transfer means higher reactivity, which lead to the formation of functional groups. Carboxylic acids, lactones, phenols and carboxyl-carbonate species are responsible for acidic properties of edge planes [10, 11, 12].

Table 3. Surface energy components of HOPG, PGB, and PGE.

	vOCG	γ^{tot}	γ^{LW}	γ^{AB}	γ^+	γ^-
pristine	HOPG	46.18	42.94	3.25	0.81	3.24
	Basal	41.80	35.93	5.87	1.01	8.54
	Edge	51.26	50.03	1.23	4.36	0.09

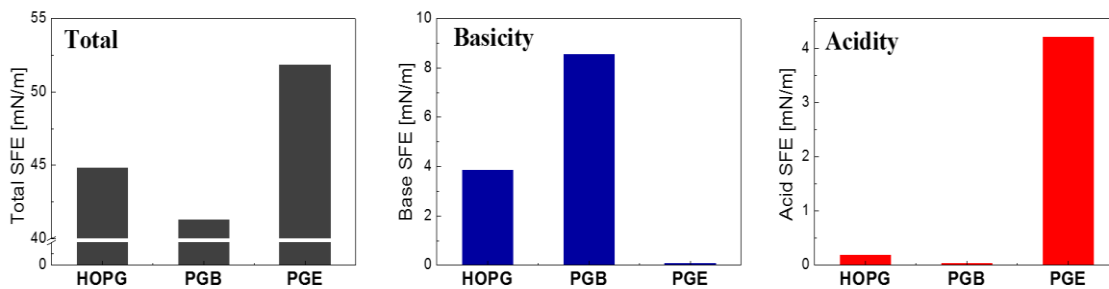


Figure 21. Surface energy components (a) total, (b) γ^- and (c) γ^+ of HOPG, PGE, and PGB electrodes.

It is noted that pure edge or basal planes are not obtainable in real experimental condition, so the SFE values of HOPG and PGB may be somewhat different to each other even they are theoretically identical systems. Based on the SFE values, we can conclude that HOPG has more edge steps than PGB because it shows higher total surface energy and lower γ^- , which resembles the SFE behavior of PGE. In other words, it seems that the HOPG used in this study contains more edge portion than PGB.

2.3.2 SFE analysis of SEI-formed edge and basal graphite

Among the three types of electrolytes, LiFSI based-electrolyte shows the highest ionic conductivity and the lowest viscosity. LiPF₆ and LiClO₄-electrolytes exhibit similar viscosity but LiPF₆ solution has higher ionic conductivity. As shown in Fig. 23, the Li insertion/deinsertion current in LiPF₆ is smallest, which is attributed to the fact that LiPF₆ forms resistive LiF-rich SEI layer. In contrast, LiClO₄ forms highly conductive organic-rich SEI layer, so LiClO₄ shows highest redox current among the three electrolytes.

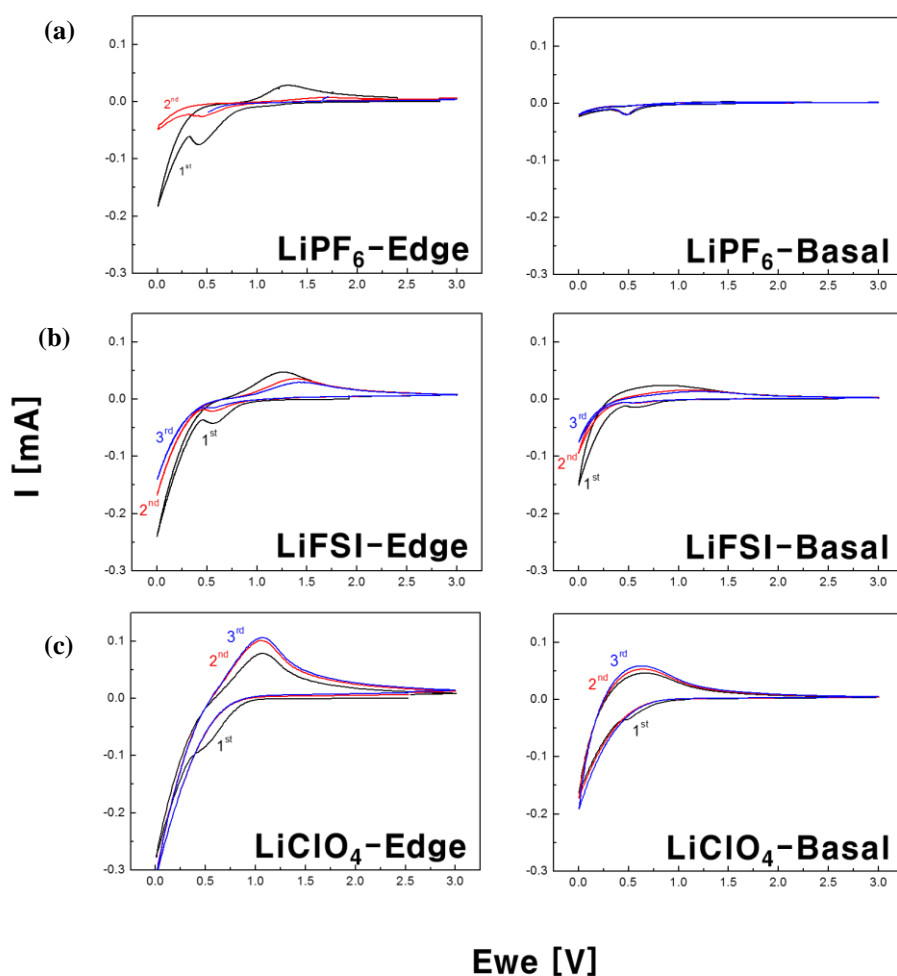


Figure 22. CVs for SEI formation in 1M (a) LiPF₆ (b) LiFSI and (c) LiClO₄ in EC/DEC

(1/2, v/v). Data form edge planes (left) and basal planes (right).

Larger redox current is observed for PGE than for PGB, which seem to be due to the preferential orientation of a PGE for Li transport. In a LiClO_4 solution, the reduction current starts to flow below 0.9 V during the 1st cathodic sweep, and an oxidation peak is observed at 1.0 V during the following anodic sweep. The reduction and oxidation currents are obviously assigned to the intercalation and the deintercalation of Li^+ ion through PGE, respectively [17-23]. No reduction current due to solid electrolyte interphase (SEI) formation is discernible during the 1st cathodic sweep. Similar voltammetric behaviors were also observed in previous reports on the edge plane of mechanically polished HOPG in LiClO_4 solutions [17-19]. However, this seems to be due to the fact that the SEI formation current overlapped with the much larger Li^+ intercalation response, since the SEI formation peak is present at a slower scan rate. The peak diminishes during the subsequent cycles; this decrease can be attributed to SEI formation [20-22]. The CV in LiPF_6 is dramatically different from that in LiClO_4 . It exhibits, during the 1st cathodic sweep, a distinct reduction peak at 0.42 V that keeps decreasing during the following cycles, which is assigned to SEI formation [21, 22]. The cur-

rent tail after the reduction peak and the oxidation peak at 1.08 V during the following anodic scan can be traced to the Li^+ transport reaction, as in the case of LiClO_4 . The current scale in LiPF_6 , however, is much smaller than that in LiClO_4 (less than one half). The reduction current starts to flow below 0.8 V at the 1st cathodic sweep, and an oxidation peak is observed at 1.2 V at the following anodic sweep.

During the 1st cathodic sweep, a distinct reduction peak at 0.42 V that keeps decreasing during the following cycles, which is assigned to SEI formation. Below equations are the reduction reactions of EC when forming the SEI.

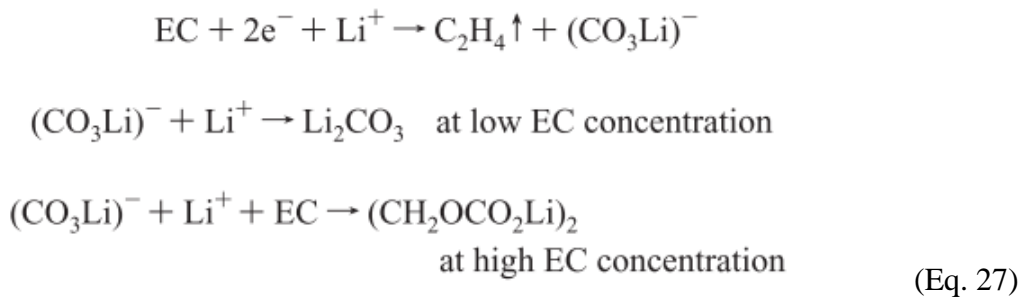


Table 1. SFE components of the graphite electrode cycled in 1 M LiPF_6 , LiClO_4 , or LiFSI solution.

	vOCG	γ^{tot}	γ^{LW}	γ^{AB}	γ^+	γ^-
Pristine	Basal	41.80	35.93	5.87	1.01	8.54
	Edge	51.26	50.03	1.23	4.36	0.09
LiPF ₆	Basal	51.16	37.12	14.05	1.17	42.01
	Edge	58.59	22.76	35.83	5.99	53.55
LiFSI	Basal	53.42	29.44	23.98	3.06	46.97
	Edge	53.58	30.87	22.71	2.97	43.43
LiClO ₄	Basal	39.98	36.80	3.18	0.04	64.02
	Edge	40.18	20.12	20.05	2.96	33.96

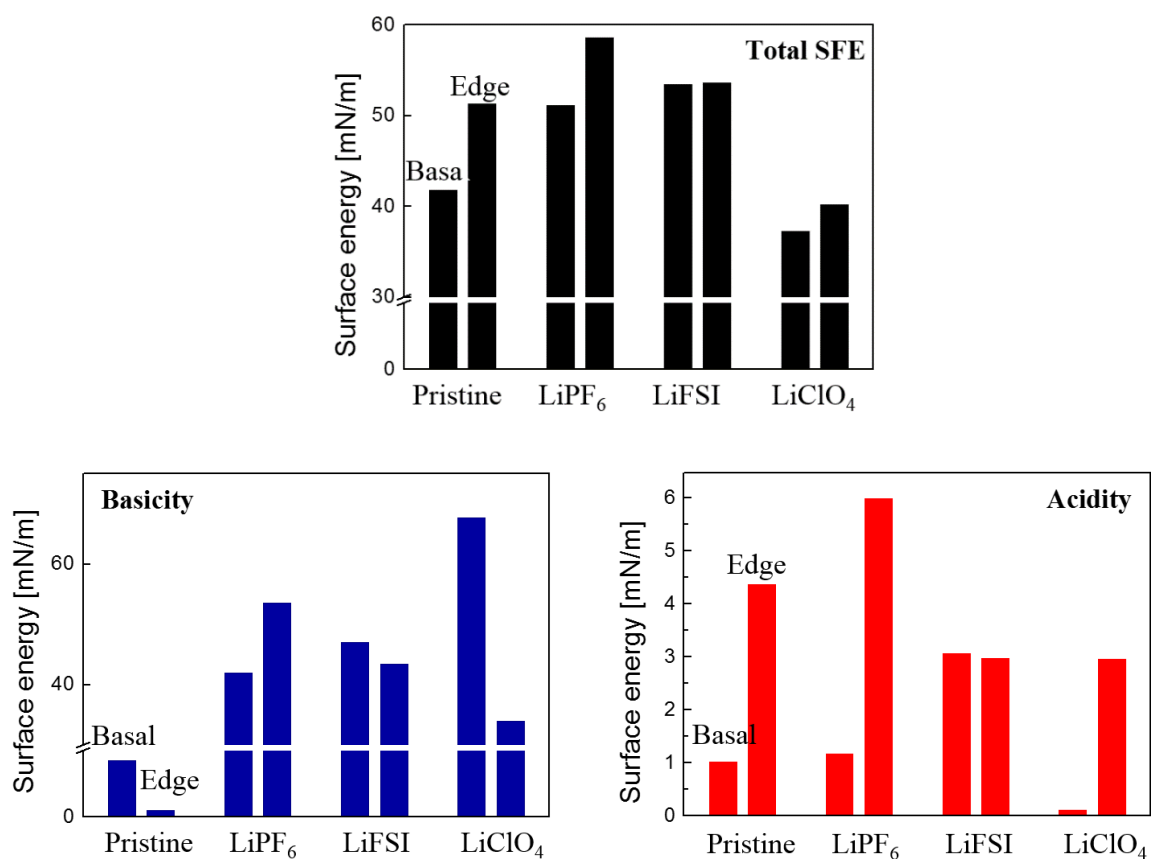
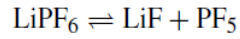
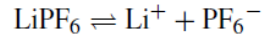


Figure 23. Total, γ^+ and γ^- values of PGE and PGB electrodes cycled in 1 M LiPF₆, LiClO₄, or LiFSI solution.

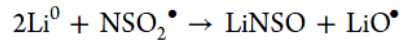
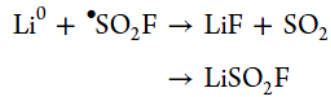
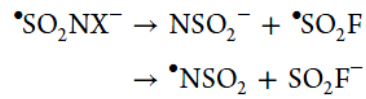
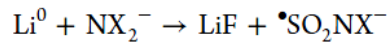
The presence of SEI layer brings dramatic difference in the SFE properties of the graphite electrodes. In particular, SEI layer greatly increases the γ^* values (from 5 to over 40 mN/m²). The origin of the dominant basicity of SEI is not clear yet, but it seems that dilithium ethylene glycol dicarbonate [(CH₂OCO₂Li)₂ : LiEDC] can be a possible reason because it is one of representative component of SEI. As shown in Fig. 21. basal plane has more polymeric material on the SEI than the cross sectional area of graphite, and salt reduction product, such as LiF, was dominant on the edge plane. For this reason, LiClO₄, which build organic-SEI film only, seems that a noticeable γ^* was observed on the basal plane. In the pristine state, shows relatively low polarity. Polishing may remove the surface functionalities. Carboxylic acids, lactones, phenols and carboxyl-carbonate species are responsible for acidic properties, where pyrone, chromene, quinone in combination with ether groups are responsible for basic properties [24].

The SFE values also depend on the types of Li salt employed for SEI formation. It is expected that LiPF₆ and LiFSI solutions form inorganic-rich SEI layer, and thus higher total SFE would be obtained. These decomposition reactions [25, 26] are in below.

LiPF₆;



LiFSI;



On the other hand, organic-rich SEI is formed in a LiClO₄ electrolyte, so that low SFE values are observed compared to LiPF₆ and LiFSI. Study of inorganic and organic material SFE in SEI layer might be a direct and convincing target of SFE difference in this study. Currently, however, cost of LiEDC became an obstacle of work.

2.4. Conclusion and future work

The SFE of pristine graphite and SEI-formed graphite was determined by sessile drop method in this work. Pristine graphite of edge and basal planes showed high γ^+ and γ^- respectively.

From this data, we may infer the acid functional groups on edge plane and abundant electrons on the basal plane. LiPF_6 , LiFSI and LiClO_4 were used as a salt to verify a SFE difference that is caused by dissimilar SEI compositions. LiPF_6 and LiFSI solutions form inorganic-rich SEI layer, and these salts made a SEI film with higher total SFEs. On the other hand, organic-rich SEI is formed in a LiClO_4 electrolyte, so lower total SFE value was observed. Regardless of salts, γ was greatly increased after SEI formation in all cases. In this study, all the contact angle measurements were performed in an ambient air condition with ca. 20-30 % relative humidity. SEI constituents are sensitive to water, so the air-exposure time has to be minimized as much as possible. Also, the model graphite system was examined in this study, so, in the future, XPS analysis will enable direct and comprehensive interpreting surface energy analysis of graphite anode and SEI-film. This does mean vOCG would have synergetic effect if we combine with atomic analysis. In brief, the following experiments will be carried out to offer more clear view on the electrochemical properties of the SEI on the graphite anode.

- (1) The humidity and exposure time control with an air conditioning to minimize the contact of water or oxygen molecules in air.
- (2) Investigation of main organic and inorganic SEI components. This will help to de-

scribe a surface energy difference of SEI film.

- (3) Coated graphite composite on a copper foil, same as real battery systems, will be employed to mimic the more realistic SEI and to perform XPS analysis.

III. Solid surface energy analysis of polymers for solid probe

3.1. Introduction

The calculation of acid–base properties by wetting measurements involves estimating the fundamental acid–base properties of solid surfaces by their ability to interact with liquids, as manifested through wetting phenomena. The basic idea of this approach [27-31] consists in the assumption that the surface free energy splits into components describing, respectively, the contribution γ^{LW} due to electrodynamic interactions (dominated by dispersion forces) and the acid–base contribution γ^{AB}

$$\gamma^{Tot} = \gamma^{LW} + \gamma^{AB} \quad (\text{Eq. 28})$$

The complementarity of acid–base interactions explicitly appears in the expression introduced by Good, van Oss and Chaudhury to describe the acid–base components the surface free energy of solids or liquids of [31-35]:

$$\gamma^{Tot} = \gamma^{LW} + 2\sqrt{\gamma^+ \cdot \gamma^-} \quad (\text{Eq. 29})$$

Combined with the Young equation and Eq. 29, leads to the following relationship for the work of adhesion between a liquid and a solid

$$W_{adh} = \gamma_i^{Tot} (1 + \cos \theta) = 2\sqrt{(\gamma_S^{LW} \cdot \gamma_i^{LW})} + 2\sqrt{(\gamma_S^+ \cdot \gamma_i^-)} + 2\sqrt{(\gamma_S^- \cdot \gamma_i^+)}$$

(Eq. 30)

From the practical point of view, equation above which will be referred to as the van Oss–Chaudhury-Good (vOCG) equation, accounts for both the acidic and the basic behavior of liquids in wetting phenomena and allows one to calculate the Lifshitz –van der Waals, the electron-donor, and the electron-acceptor parameters of a solid by contact angle measurements using (at least) three liquids of known surface free energy components.

The vOCG equation is, in principle, the tool which allows us to measure the acid–base properties of polymer surfaces, to account for the results of interfacial interactions, and to design a given surface modification treatment for a given application, but its practical use shows that it is still very far from this goal.

The characterization and quantitative description of forces at interfaces constitute one of the most important problems in materials surface and interfacial science. Its solution would make possible the analytical prediction and explanation of the materials behavior at interfaces by the quantification of interfacial interactions and, as an immediate consequence, the technological capability to design material or surface structures for a specific purpose on the basis of a precisely defined surface structure / properties relationship.

Among the different definitions of acids and bases, the Lewis theory is the most satisfactory for applications to polymers. Any substance capable of furnishing electron density must be considered a base, while an acid is any substance available to accept electron density. According to the preceding definition, the sites that can act as electron acceptors are acidic: metal atoms of organometallic compounds, electrophilic carbons (i.e. carbon atoms covalently linked to a more electronegative element, such as oxygen or fluorine), hydrogen atoms in hydroxyl or carboxyl groups. In contrast, Lewis bases are electron donors: atoms containing lone-pair electrons (such as oxygen), or aromatic rings, where the π electrons act as a basic site. This broader definition best describes the kind of acid–base interactions of interest in polymer surface and interfacial science. And it is within this same notion that the terms ‘electron donor’ and ‘electron acceptor’, and are frequently used in the literature as synonyms for ‘Lewis base’ and ‘Lewis acid’, respectively.

The individual contributions to the liquid surface tension are known for a few standard liquids. Therefore by measuring the equilibrium contact angles of (at least) three contacting liquid droplets, the three unknowns of solid surface energy can be obtained by solving a linear system of three equations $[A][x]=[b]$, given by matrix below.

$$\begin{pmatrix} \gamma_{1,1}^{\text{Tot}}(1 + \cos \theta_1)/2 \\ \gamma_{1,2}^{\text{Tot}}(1 + \cos \theta_2)/2 \\ \gamma_{1,3}^{\text{Tot}}(1 + \cos \theta_3)/2 \end{pmatrix} = A \begin{pmatrix} \sqrt{\gamma_s^{\text{LW}}} \\ \sqrt{\gamma_s^-} \\ \sqrt{\gamma_s^+} \end{pmatrix} \quad (\text{Eq. 31})$$

The relative error in the contact angle measurements (the right hand side of matrix equation) is amplified by the condition number of matrix [A], therefore the contacting liquids are chosen such that the matrix [A] is not ill-conditioned or it has as low a condition number as possible. [36,37] Condition number was defined to evaluate the triplet's sensitivity of data errors.

$$Cn = \|A\|_1 \cdot \|A^{-1}\|_1 \quad (\text{Eq. 32})$$

We has 7 probe liquid, and these were evaluated suitability of liquid triplet by a condition number. Among the triplets in the Table, we chose Wa-FA-MI triplet because it has one of lowest condition number and has measuring convenience.

Table 2. Condition numbers by 3 liquid combination. [Abbreviation] Wa : water, FA : formamide, MI : diiodomethane, Gly : glycerol, BN : 1-bromonaphtalene, DMSO : dimethylsulfoxide, EG : ethyleneglycol

Triplet	C. N.	Triplet	C. N.
Gly-Wa-EG	31.687	Gly-DMSO-BN	30.25
FA-Gly-BN	175.688	FA-Gly-Wa	25.46

FA-Wa-DMSO	119.84	Wa-DMSO-EG	133.43
Gly-DMSO-EG	46.42	Gly-Wa-DMSO	19.99
FA-EG-BN	54.58	Wa-FA-MI	7.54
FA-Gly-EG	67.58	Wa-Gly-MI	6.30
Gly-EG-BN	75.6	Wa-Gly-BN	6.13
FA-DMSO-EG	343.98	Wa-FA-BN	7.35
DMSO-EG-BN	22.01	Wa-DMSO-MI	7.19
FA-Gly-DMSO	78.17	Wa-DMSO-BN	7.00
FA-DMSO-BN	36.06	Wa-EG-BN	8.91

For a simple example of condition number, contact angle of 7 probe liquid were measured on a PET film. Various triplets were made to calculate PET surface energy, but only when condition number is appropriate, surface energy was acceptably deduced. In a figure below, large error was found in higher condition number, and lower condition number that is below 10 deduced a much proper total surface energy of solid.

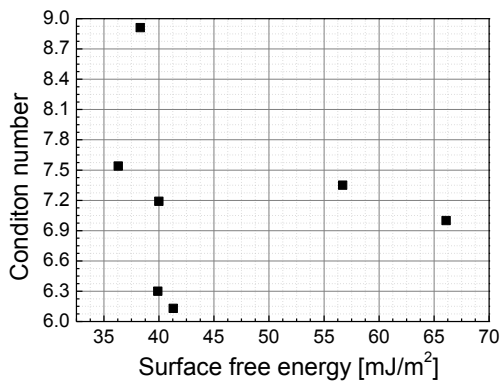
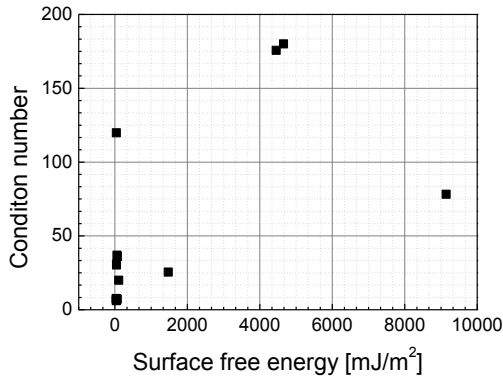


Figure 24. High condition number (left) and low condition number triplet (right) for solid surface energy measurements.

Many factors affect the electrochemical performances of lithium-ion batteries. The wettability of the porous electrodes in such cells by the electrolyte is related to capacity and high-rate discharge ability. For example, wetting in a porous electrode with very small pores is problematic, and most of the surface area may not be wetted [38-41]. This results in poor utilization of electrode capacity. In addition, the electrolyte resistance may be increased, thus handicapping high current charging and discharging current. Menachem et al. [39] used the burn-

off method to modify graphite powder. After treatment, these modified graphites showed better wetting. Furthermore, Manev et al. [40] examined the influence of compacting pressures at electrode preparation on discharge capacity. Experimental results showed that increasing the pressing time leads to a decrease in discharge capacity. This is believed to be due to incomplete wetting of the electrode by lowering the electrode porosity [40, 41]. It is thus important to improve the contacting behavior of the electrode–electrolyte interface in porous electrodes. However, only a few studies mention the effects of electrode porosity or particle size on the wetting in lithium-ion batteries.

In this study, 3 component of solid surface energy were defined by advancing contact angle measurement. Contact angles of 3 liquids were measured on 7 polymers. Based on a vOCG theory, we deduced 3-component solid surface energy and condition numbers.

3.2. Experimental

The contact angles were determined using the following reference liquids: Ultra-pure water (W), Formamide (F) (HCONH_2 , 99.5% Reagent grade, Alfa aser), Diiodomethane (D) (CH_2I_2 , 99% stab., Alfa aser). The letters W, F and D were used to stand for relevant reference liquids

and the corresponding contact angles are quoted as W, F and D, respectively for water, formamide and diiodomethane at the air, liquid, solid interface. The values of SFE of the reference liquids and its components, used for the calculations, are displayed in Table 1.

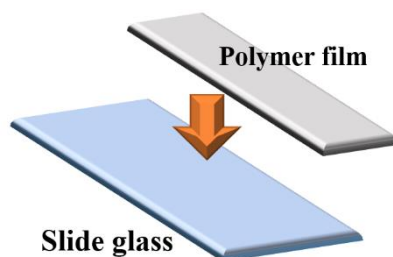


Figure 25. Polymer sample preparing for contact angle measurement.

Smooth polymeric materials (Goodfellow, Cambridge) were used for the characterization of the solid surface energy: polyethylene (PE), polypropylene (PP), polyvinylfluoride (PVF), polybutylene terephthalate (PBT), polymethyl methacrylate (PMMA), polystyrene (PS), polyvinyl chloride (PVC). Polymers were cut out to attach on the slide glass. This helps the washing precursor and contact angle measurement. Then polymer samples were sonicated with a detergent, ethanol and DI water, in the order, and dried with a nitrogen gun.

The contact angles (CA) were measured according to the advancing angle method using a DSA100 goniometer (Krüss, Germany), at room temperature (25 ± 2 °C). Dynamic contact

angle measurements (i.e., advancing and receding contact angles) can be performed by adjusting the volume of the drop from above or below the solid surface. However, if it is adjusted from the top, its profile will be disturbed as the needle pierces the drop. Since ADSA requires a complete drop profile for determining contact angles, liquid has to be supplied from the bottom of the drop. Therefore, liquid is pumped into or withdrawn from the drop by a motorized syringe through a small hole in the solid surface. The procedure allows measurement of the contact angles without disturbing influences, such as the vibration of the drops. It has been shown that contact angles on well-prepared solid surfaces are independent of the rate of the advancing at moderate rates up to at least 1 mm/min. In other words, low-rate dynamic contact angles are identical to the static contact angles.

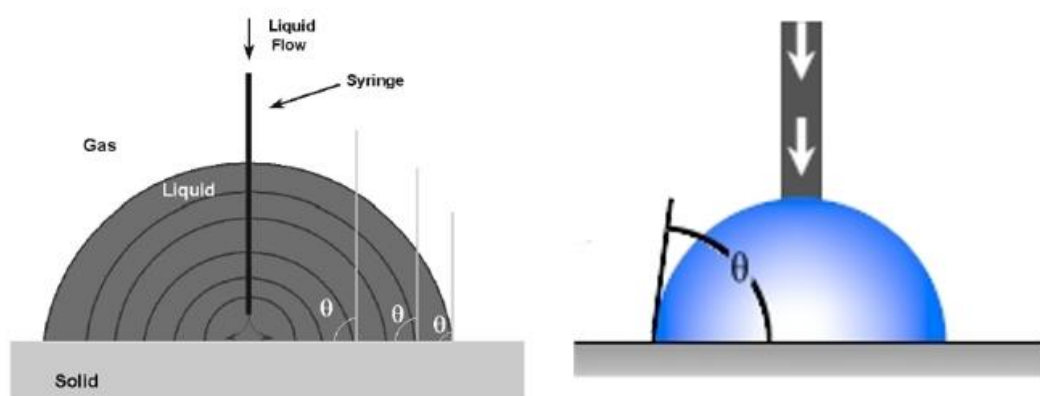


Figure 26. Schematic view of advancing angle measurement.

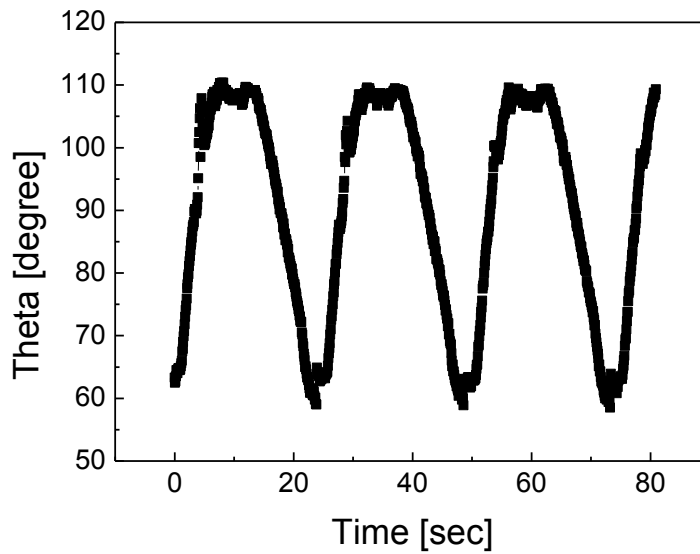


Figure 27. Typical advancing angle measurement time-contact angle graph. This data is from water contact angle on PE film.

3.3. Results

Advancing angle data on polymer films are in a Table. Except for few cases such as MI angle on PBT and Wa angle on PVC film, advancing angle data was generally reproducible and quite stable.

Table 6. Advancing angle data (first advancing angle/ second advancing angle).

	Wa	Fa	MI
PTFE	-/122	-/102	-/95
PP	99/95	85/79	60/60
PE	102/105	84/85	51.5/58
PVF	82/83	61/61.5	48/48
PBT	98/87	70/75	38/56
PMMA	80/79.5	69/67	44/45

PS	92/93	80/73	Miscible
PVC	87/77	65/65	40/40.5

However, reported contact angle was also considered to exclude exceptional data errors. In some paper, even they used same material, like PMMA and FA, contact angles were somewhat different. This states that in our experiment could have a difference although material itself was called as a same name. Impurity, pretreatment or sample storage condition may differ the surface property. Therefore, in an experimental error, we referred a reported data for fair surface energy calculation.

Table 7. Advancing angle data that are reported from C. Della Volpe and Wu. (): data from Wu. Underlined data are one of closest measured value with the reported one [36 , 41].

	Wa	Fa	MI
PTFE	114.6	91.16	73.94
PP	107.73	<u>80.35</u>	<u>58.57</u>
PE	103.13 (<u>102</u>)	72.70-76.14 (77)	46.32 (<u>53</u>)

PVF	<u>83.67</u> (80)	48.94-46.8 (54)	46.69 (<u>49</u>)
PBT	79.62	39.29-36.73	35.06- <u>36.73</u>
PMMA	87.42 (80)	44.04-41.05 (<u>64</u>)	37.18 (<u>41</u>)
PS	<u>91.87</u> (91)	56.38-57.71 (<u>74</u>)	36.34 (35)
PVC	90.377 (<u>87</u>)	51.31-51.48 (<u>66</u>)	33.75 (<u>36</u>)

Table 8. Solid surface energy by measuring advancing angle measurements.

	γ^{tot}	γ^d	γ^P	γ^-	γ^+
PTFE	10.64	10.58	0.06	0.01	0.18
PP	24.21	23.43	0.78	0.67	0.22
PE	31.52	31.45	0.07	0.03	0.04
PVF	36.77	34.83	1.94	1.70	0.55
PBT	40.62	40.60	0.02	0.05	0.00
PMMA	39.96	39.10	0.86	2.47	0.07
PS	41.99	41.56	0.43	0.49	0.09
PVC	41.79	41.56	0.23	0.94	0.01

Solid surface energy was calculated using Wa-FA-MI triplet based on a vOCG theory. For the

further utilization of polymer surface energy was calculated and tabled below.

Table 9. Screened solid triplets which has condition number less than 65.

Combination	C.N.
PTFE-PP-PVC	60.72
PTFE-PE-PVC	60.21
PTFE-PE-PMMA	39.13

PTFE-PVF-PVC	63.26
PTFE-PVF-PMMA	56.83
PTFE-PBT-PMMA	43.01
PTFE-PVF-PMMA	64.00
PP-PVF-PMMA	41.29
PE-PVF-PMMA	37.57
PVF-PBT-PMMA	38.63
PVF-PMMA-PS	41.10
PVF-PMMA-PVC	45.47

3.4. Discussion and future plan

Polymer surface energy was calculated by measuring advancing angles on the polymer. Combination of well-conditioning solid triplets may help to find a battery electrolyte. If well-conditioned solid triplet would be found, an accuracy can be tested by a probe liquid evaluation, because we already know a liquid 3-component surface energy. In other words, comparing calculated liquid surface energy by solid triplet and conventional liquid 3-component surface energy is one way to check a correctness of solid surface energy. One more thing to be improved is about higher solid surface energy than a liquids. When liquid total surface energy is much lower than solid substrate, liquid tend to cover the solid to stabilize the system. This

means that contact angle cannot be detected because liquid is going to be spread out of the solid surface. Therefore, solid with lower surface energy is preferable if possible. Also, encasing gel- method could be cooperated to have accurate 3-component surface energy of probe liquid.

References

- [1] H. Dipl.-Phys. Hubert Lechner. Krüss, Germany (1996) 110-115.
- [2] E.W. Washburn, Physical Review, 17 (1921) 273-283.
- [3] A. Lundblad, B. Bergman, J Electrochem Soc, 144 (1997) 984-987.
- [4] C. Bakli, S. Chakraborty, Appl Phys Lett, 101 (2012) 103-112.
- [5] Cookson J.T., Carbon adsorption Handbook, 3rd ed., Ann Arbor Science (1978) p241-253.
- [6] Pierson H.P., Handbook of Carbon, Graphite, Diamond and Fullerenes, fourth ed., Noyes, (1993) 269-290.
- [7] D. Bar-Tow, E. Peled, and L. Burstein, J. Electrochemical Soc., 146 (1999) 824-832.
- [8] Perla B. Balbuena, Yixuan Wang, Lithium ion batteries: Solid-electrolyte interface, Ed., World Scientific (2004) 66-129.
- [9] Kang Xu, Chem. Rev. 104 (2004) 4303-4417.
- [10] C. Della Volpe et.al. J. of Adhesion Science and Technology, 14:2 (2000) 235-272
- [11] M. Ochida, Y. Domi, T. Doi, S. Tsubouchi, H. Nakagawa, T. Yamanaka, T. Abe, Ogumi, J. Electrochem. Soc 159 (2012) A961-A966.
- [12] Le Yu, Huijin Liu, Yan Wang, Naoaki Kuwata, Masatoshi Osawa, Junichi Kawamura, and Shen Ye, Angew. Chem., 52 (2013) 1-5
- [13] Wu S. polymer Interface and Adhesion, Marcel Dekker Inc., (1982) 280-312
- [14] Collins J, Zheng D, Ngo T, Qu D, Carbon (2014) 79, 500-17.
- [15] Collins J, Ngo T, Qu D, Foster M., Carbon (2013) 57,174-83.
- [16] Moreno-Castilla C., Carbon 42 (2004) 83-94.
- [17] M. Ochida, Y. Domi, T. Doi, S. Tsubouchi, H. Nakagawa, T. Yamanaka, T. Abe, Ogumi, J. Electrochem. Soc 159 (2012) A961-A980.
- [18] Y. Domi, M. Ochida, S. Tsubouchi, H. Nakagawa, T. Yamanaka, T. Domi, T. Abe, Z. Ogumi, J. Electrochem. Soc., 159 (2012) A1292-A1297
- [19] X. Wang, K. Aoki, J. Electrochem. Soc., 604 (2007) 101-132.

- [20] F.P. Campana, R. Kotz, J. Vetter, P. Novak, H. Siegenthaler, *Electrochem. Comm.* 7 (2005) 107.
- [21] M. Tang, K. Miyazaki, T. Abe, J. Newman, *J. Electrochem. Soc.* 159 (2012) A634-A678.
- [22] M. Tang, J. Newman, *J. Electrochem. Soc.* 159 (2012) A1922-A1988.
- [23] H. Nakarawa, Y. Domi, T. Doi, M. Ochida, S. Tsubouchi, T. Yamanaka, T. Abe, Z.Ogumi, *J. Power Sources* 236 (2013) 138-144.
- [24] John Collins, Gerald Gourdin, Michelle Foster, Deyang Qu, *Carbon* 92 (2015) 193-244
- [25] Tetsuya Kawamura, Shigeto Okada, Jun-ichi Yamaki, *J. Power Sources* 156 (2006) 547-554
- [26] Ilya A. Shkrob, Timothy W. Marin, Ye Zhu, and Daniel P. Abraham, *J. Physical Chemistry C* 118 (2014) 19661-19671
- [27] F. M. Fowkes, in: *Physicochemical Aspects of Polymer Surfaces*, K. L. Mittal (Ed.), Vol. 2, Plenum Press, New York (1983) 583-603.
- [28] F. M. Fowkes, in: *Surface and Interfacial Aspects of Biomedical Polymers*, J. D. Andrade (Ed.), Vol. 1, Plenum Press, New York (1985) 337-372.
- [29] F. M. Fowkes, *J. Adhesion Sci. Technol.* 1, (1987) 7-27.
- [30] J. C. Berg, in: *Wettability*, J. C. Berg (Ed.), Ch. 2. Marcel Dekker, New York (1993) 60-90.
- [31] R. J. Good and M. K. Chaudhury, in: *Fundamentals of Adhesion*, L. H. Lee (Ed.), Ch. 3. New York, Plenum Press (1991) 129-250.
- [32] C. J. van Oss, R. J. Good and M. K. Chaudhury, *J. Protein Chem.* 5, (1986) 385-402.
- [33] C. J. van Oss, M. K. Chaudhury and R. J. Good, *Adv. Colloid Interface Sci.* 28, (1987) 35-60.
- [34] R. J. Good and C. J. van Oss, in: *Modern Approach to Wettability, Theory and Application*, M. E. Schrader and G. Loeb (Eds), Plenum Press, New York (1991) 1-28.
- [35] C. J. van Oss, *Interfacial Forces in Aqueous Media*. Marcel Dekker, New York (1994) 259-271.
- [36] Volpe, C. D.; Siboni, S. J. *Colloid Interface Sci.* 195 (1997) 121-136.
- [37] Shalel-Levanon, S.; Marmur, A. J. *Colloid Interface Sci.* 262 (2003) 489-499.
- [38] V. Manev, I. Naidenov, B. Puresheva, P. Zlatilova and G. Pistoia, *J. Power Sources* 55 (1995) 122-140
- [39] C. Menachem, E. Peled, L. Burstein and Y. Rosenberg, *J. Power Sources* 68 (1997) 211-220

[40] V. Manev, I. Naidenov, B. Puresheva and G. Pistoia, *J. Power Sources* 57 (1995) 277-290

[41] P. Novaćk, W. Scheifele, M. Winter and O. Hass, *J. Power Sources* 68 (1997) 267-278.

요 약 문

전극 및 전해질 물질의 표면에너지와 리튬 이온 전지 성능의 상관관계 연구

시장의 전자기기와 전기자동차에 대한 큰 수요에도 불구하고, 전극/전해질 계면의 근본적인 이해는 아직 밝혀져야 할 부분이 많다. 계면현상은 전극의 표면과 전해액의 물리화학적 특성에 의해 결정된다.

본 연구의 첫 번째 단원에서는, 다양한 상용 등급의 LiMn_2O_4 (이하 LMO)의 표면자유에너지(이하 SFE)를 van Oss-Chaudhary-Good (이하 vOCG) 이론을 바탕으로 분석하여 Lifshitz van der Waals (γ_s^{LW}), 산 (γ_s^+), and 염기 (γ_s^-) 로 구분하였다. Mn 용출 현상은 short-range coulombic force와 관련된 산-염기 표면에너지와 강하게 연관된 것으로 드러났다. LMO 표면의 산 자리와 전해액의 염기 성질 (e.g., solvents, anions), 그리고 전극의 염기 자리와 전해질의 산 성질 (e.g., HF)은 서로 단거리 coulomb 힘으로 상호작용 하는 경향을 보인다.

두 번째 단원에서는 흑연전극과 흑연전극에 형성된 Solid electrolyte interface(이하 SEI) 층의 SFE 를 통해 표면 화학 종을 간접분석 하였다. 흑연전극의 Edge 와 basal 면은 각각 γ^+ 와 γ^- 가 높게 나왔다. SEI 층은 흑연전극의 SFE 를 크게 바꾸는데, 특히 γ^- 값은 10 배 가량 증가한다. 또한, SFE 값은 SEI 층 형성에 쓰인 Li 염의 종류에도 영향을 받는다. LiPF_6 와 LIFSI 용액은 주로 무기물 SEI 층을 형성하고, 그에 따라 LiClO_4 용액이 형성한 유기물 SEI 층 보다 높은 SFE 를 보였다.

세 번째 단원에서는 낮은 condition number 를 가진 고체조합을 찾기 위하여 다양한 고분자 기판을 조사하였다. Condition number 는 액체 혹은 고체 조합의 적합도를 평가하는 데 필수적인 척도이다. 현재의 액체조합 보다는 높지만, PE/PVF/PMMA 는 가장 낮은 condition number 를 보였다. 더 좋은 고체조합을 찾기 위한 추가적인 탐색이 필요하다.

핵심어: 표면자유에너지, LiMn_2O_4 , 금속용출, 흑연전극, SEI, condition number